AD-A068 733 TEXAS UNIV AT AUSTIN APPLIED RESEARCH LABS F/G 20/1
ASPECTS OF THE ACOUSTIC BOTTOM INTERACTION PROBLEM.(U)
DEC 78 K E HAWKER N00039-77-C-0003
UNCLASSIFIED ARL-TR-78-49 NL

| OF |
AD
A068733

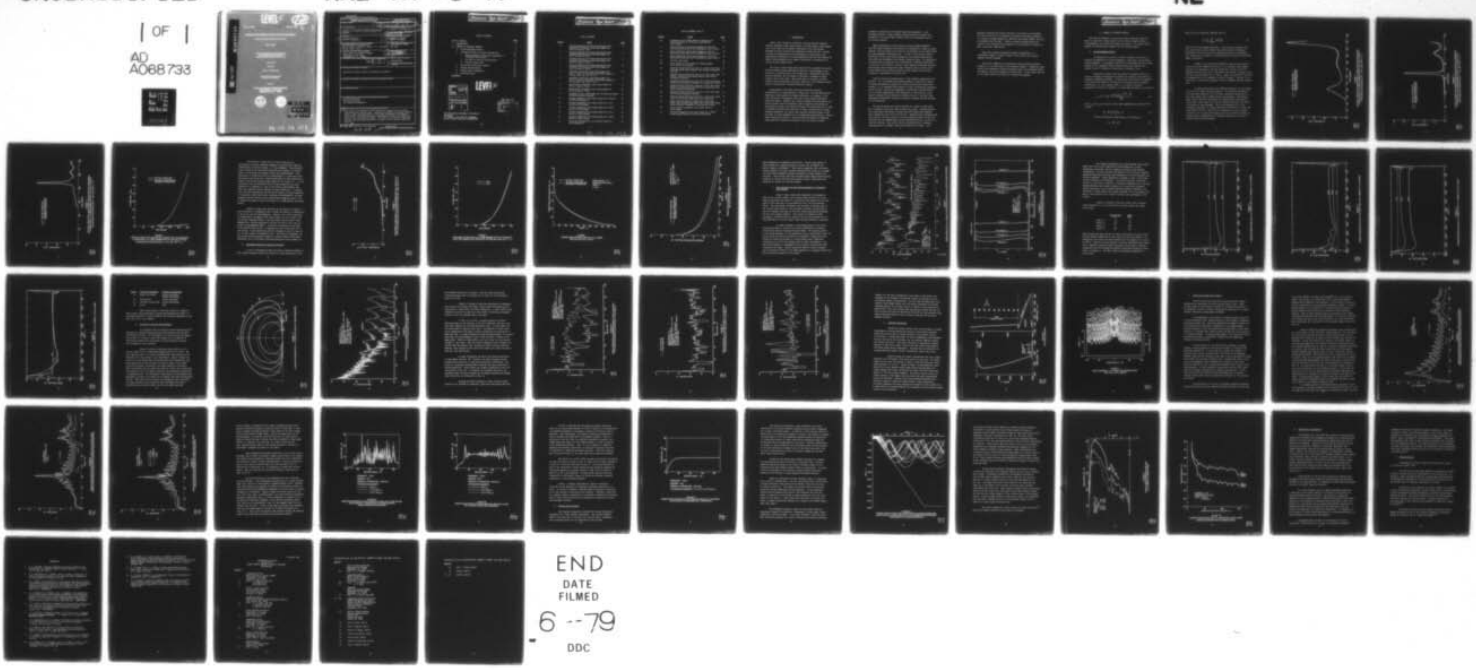

END
DATE
FILMED
6 -79
DDC

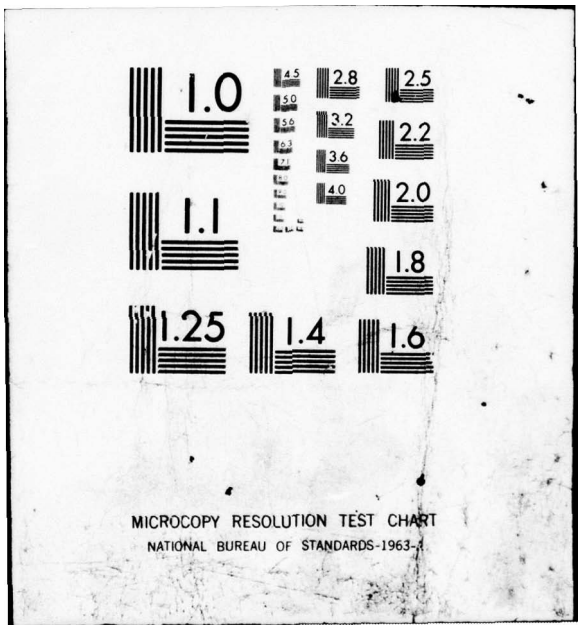
1.0
1.1
1.25
1.4
1.6
1.8
2.0
2.2
2.5
2.8
3.2
3.6
4.0
4.5
5.0
5.6
6.3
MICROCOPY RESOLUTION TEST CHART
NATIONAL BUREAU OF STANDARDS-1963-A

LEVEL II

ARL-TR-78-49

Copy No. 18

ASPECTS OF THE ACOUSTIC BOTTOM INTERACTION PROBLEM

Final Report under Contract N00039-77-C-0003, Item 0001

Kenneth E. Hawker

APPLIED RESEARCH LABORATORIES
THE UNIVERSITY OF TEXAS AT AUSTIN
POST OFFICE BOX 8029, AUSTIN, TEXAS 78712

7 December 1978

Final Report

10 January - 30 December 1977

APPROVED FOR PUBLIC RELEASE:
DISTRIBUTION UNLIMITED.

Prepared for:

NAVAL ELECTRONIC SYSTEMS COMMAND
DEPARTMENT OF THE NAVY
WASHINGTON, D. C. 20360

79 05 09 011

UNCLASSIFIED

SECURITY CLASSIFICATION OF THIS PAGE (When Data Entered)

REPORT DOCUMENTATION PAGE

READ INSTRUCTIONS BEFORE COMPLETING FORM

1. REPORT NUMBER

2. GOVT ACCESSION NO.

3. RECIPIENT'S CATALOG NUMBER

(9) Final rept. 10 Jan-31 Dec 77

4. TITLE (and Subtitle)

(6) ASPECTS OF THE ACOUSTIC BOTTOM INTERACTION PROBLEM

5. TYPE OF REPORT & PERIOD COVERED

technical report

6. PERFORMING ORG. REPORT NUMBER

(14) ARL-TR-78-49

7. AUTHOR(s)

(10) Kenneth E. Hawker

8. CONTRACT OR GRANT NUMBER(s)

(15) N00039-77-C-0003

9. PERFORMING ORGANIZATION NAME AND ADDRESS

Applied Research Laboratories
The University of Texas at Austin, P. O. Box 8029
Austin, Texas 78712

10. PROGRAM ELEMENT, PROJECT, TASK AREA & WORK UNIT NUMBERS

Item 0001

11. CONTROLLING OFFICE NAME AND ADDRESS

(11) Naval Electronic Systems Command
Department of the Navy
Washington, D. C. 20360

12. REPORT DATE

7 December 1978

13. NUMBER OF PAGES

52

14. MONITORING AGENCY NAME & ADDRESS (if different from Controlling Office)

(12) 59 p.

15. SECURITY CLASS. (of this report)

UNCLASSIFIED

15a. DECLASSIFICATION/DOWNGRADING SCHEDULE

16. DISTRIBUTION STATEMENT (of this Report)

Approved for public release; distribution unlimited.

17. DISTRIBUTION STATEMENT (of the abstract entered in Block 20, if different from Report)

18. SUPPLEMENTARY NOTES

19. KEY WORDS (Continue on reverse side if necessary and identify by block number)

bottom interaction
sea floor acoustics
low frequency propagation

20. ABSTRACT (Continue on reverse side if necessary and identify by block number)

(U) This report is a synopsis of work carried out during 1977 on acoustic interaction with the sea floor. Results are reported concerning roughness effects, mode stripping effects on the depth dependence of propagated sound fields, vertical directivity consideration, bottom loss sensitivity studies, and other related studies. The bulk of the material summarized here has been previously reported in original form in various papers and reports.

DD FORM 1 JAN 73 1473 EDITION OF 1 NOV 65 IS OBSOLETE

UNCLASSIFIED

SECURITY CLASSIFICATION OF THIS PAGE (When Data Entered)

404 434

TABLE OF CONTENTS

LIST OF FIGURES

LIST OF FIGURES (Cont'd)

I. INTRODUCTION

Under a wide variety of conditions of source-receiver geometry, acoustic frequency, sound speed profile, and water depth, sound propagation in the ocean can be heavily influenced by the ocean bottom. Although sea floor structure and composition itself has been a subject for study by geophysicists and seismologists for many years, only comparatively recently has it been appreciated that sea floor makeup can impact sound propagation over ranges, frequencies, and geometries of concern to Naval applications.

The scope of these applications which must be concerned with bottom effects includes system performance prediction, system design, interpretation of acoustical data, the integration of geophysical data into acoustic modeling, and the design of experiments intended to gather acoustic data in the ocean. This broad range of concerns for which acoustic bottom interaction can play a significant role requires various levels of description of bottom interaction effects.

Traditionally, the nature of bottom interaction has been characterized by a single quantity, bottom loss. For many applications knowledge of this quantity is indeed sufficient, for example, in ray trace estimates of propagation loss used in some system performance prediction models. However, more complex problems involving phase interference between various multipaths, such as questions concerning the functioning of arrays, the nature of Doppler line broadening, and a range of problems concerned with multipath, or mode, conversion due to range changing bathymetry, all require more detailed characterization of the sea floor if these phenomena are to be understood quantitatively. Many of these problems may require a fairly detailed description of subbottom sound speed and attenuation profiles as well as location of major

interfaces (reflectors) and possibly shear wave parameters. Such problems go beyond a simple regional characterization of bottom loss estimated in 1/3 octave bands, however useful such information may be for certain problems.

Under sponsorhsip of Naval Electronic System Command (NAVELEX) Code 320, Applied Research Laboratories, The University of Texas at Austin (ARL:UT), has been conducting a study of the influence of the ocean bottom on sound propagation characteristics. In view of the various levels of description of the ocean bottom required by the intended applications, this study has encompassed three primary technical areas: (1) sensitivity of bottom loss to variations and uncertainties in subbottom parameters, (2) the role of the bottom in various range changing environment problems, particularly slope coupling and bottom roughness, and (3) bottom interaction effects such as those involved in array studies and the interpretation of experimental acoustical data.

From the outset the primary goals of this research program have been fourfold: (1) to determine and provide guidance on the level of detail of subbottom parameters required for acoustic applications (sensitivity studies), (2) to determine which aspects of mode, or multipath, conversion caused by slope coupling and roughness are predictable and exploitable, (3) to develop computational tools appropriate to the study of a wide range of complex bottom interaction problems, and (4) to interact with experimental measurement programs via exercise planning and data analysis and interpretation.

The various papers and reports produced as a result of this study have a bearing on the first three of these four goals. Interaction with both experimental measurement programs and other exploratory development programs has been active and fruitful. Modeling tools developed under this contract have been used in a new data reduction method for SUS data developed for the BEARING STAKE exercise (NOSC/PME-124-60), as well as in exercise planning. This effort has been described fully in numerous briefings given to NAVELEX, Codes 320 and PME-124 and others. Both

modeling techniques and results obtained in the course of the present study have been used in the analysis of ambient noise depth dependence in a research program sponsored at ARL:UT by both LRAPP (NORDA, Code 600) and NAVELEX, Code 320 (NRL). Finally, methods developed during the course of this study have been employed in the interpretive analysis of RDSS related data (PME-124-30).

Thus, this research program has already accomplished, to a considerable degree, a useful transfer of its results into various systems oriented programs.

This report summarizes the principal technical results obtained during FY 77, the third year of this research program. Inasmuch as these results are documented in either existing or soon to be published papers and reports, only brief summaries are given here. In most cases only one or two sample results are given for illustrative purposes.

II. SUMMARY OF PRINCIPAL RESULTS

This section summarizes the principal results obtained during the course of this work. These results are (1) bottom roughness effects, (2) propagation, (3) bottom loss sensitivity studies, (4) sloping bottom studies, (5) shallow water studies, and (6) modeling support.

A. Bottom Roughness Effects

The objective of the work on bottom roughness effects was to estimate the importance of bottom roughness to long range, low frequency sound propagation. A secondary objective was to determine whether a viable approach to the roughness problem existed which would require only a minimal amount of information concerning the roughness itself.

During this contract year the theory of roughness effects on acoustic propagation developed by Kuperman[1] was applied to deep water low frequency propagation problems. In this theory, the effects of roughness on the mean field appear as corrections to the normal mode attenuation coefficients, δ_n. The acoustic field, ϕ, at range r and depth z generated by a source of frequency ω at zero range and depth z_o is given by

$$\phi = e^{-i\pi/4} \frac{1}{\sqrt{2\pi}} \frac{U_n(z)U_n(z_o)\, e^{ik_n r}\, e^{-\delta_n r}}{\sqrt{k_n r}} \quad , \tag{1}$$

where k_n and U_n are the usual normal mode eigenvalues and eigenfunctions obeying

$$U_n'' + \left(k^2(z) - k_n^2\right) U_n = 0 \quad . \tag{2}$$

The mode attenuation coefficients δ_n are written as

$$\delta_n = \delta_n^a + \delta_n^s \quad , \tag{3}$$

where δ_n^a is the absorption component given by

$$\delta_n^a = \frac{\omega}{k_n} \int_{sed} dz U_n^2 \left(\frac{\alpha}{c}\right) \quad , \tag{4}$$

where $\alpha(z)$ is the sediment absorption. The scattering component δ_n^s is the quantity given by the boundary perturbation theory of Kuperman. Calculations of both δ_n^s and the accompanying effects on transmission loss (some aspects of which are reproduced here) are given by Rutherford, Hawker, and Payne.[2]

Figures 1 and 2 show δ_n^a and $\delta_n^a+\delta_n^s$ for clay and sand layers at 20 Hz with an rms roughness value of 5 m. As intuition would suggest, the effect of roughness on the mode attenuation is less for the low impedance contrast clay than for the harder sand bottom. Figures 3 and 4 show the same situations, but at 100 Hz. Again, the effects of this level of roughness for a clay sediment are seen to be small. However, in the sand case, at 100 Hz, the roughness is seen to dominate the mode attenuation.

In these calculations, the sediment absorption, α, was assumed to obey a first power law with frequency. The frequency dependence of the scattering component, δ_n^s, of the mode attenuation coefficients is much more complex and no simple results are available. Nevertheless, these results show that the effects of roughness grow with frequency faster than a first power law, and will therefore overwhelm the absorption effects at some frequency. For an rms roughness of 5 m this "crossover" frequency is clearly between 20 Hz and 100 Hz for sand, and above 100 Hz for clay. This value of roughness was chosen, somewhat arbitrarily, to be sufficiently small so as to be within the domain of irregularities encompassed by the roughness problem, not the deterministic sloping bottom problem.

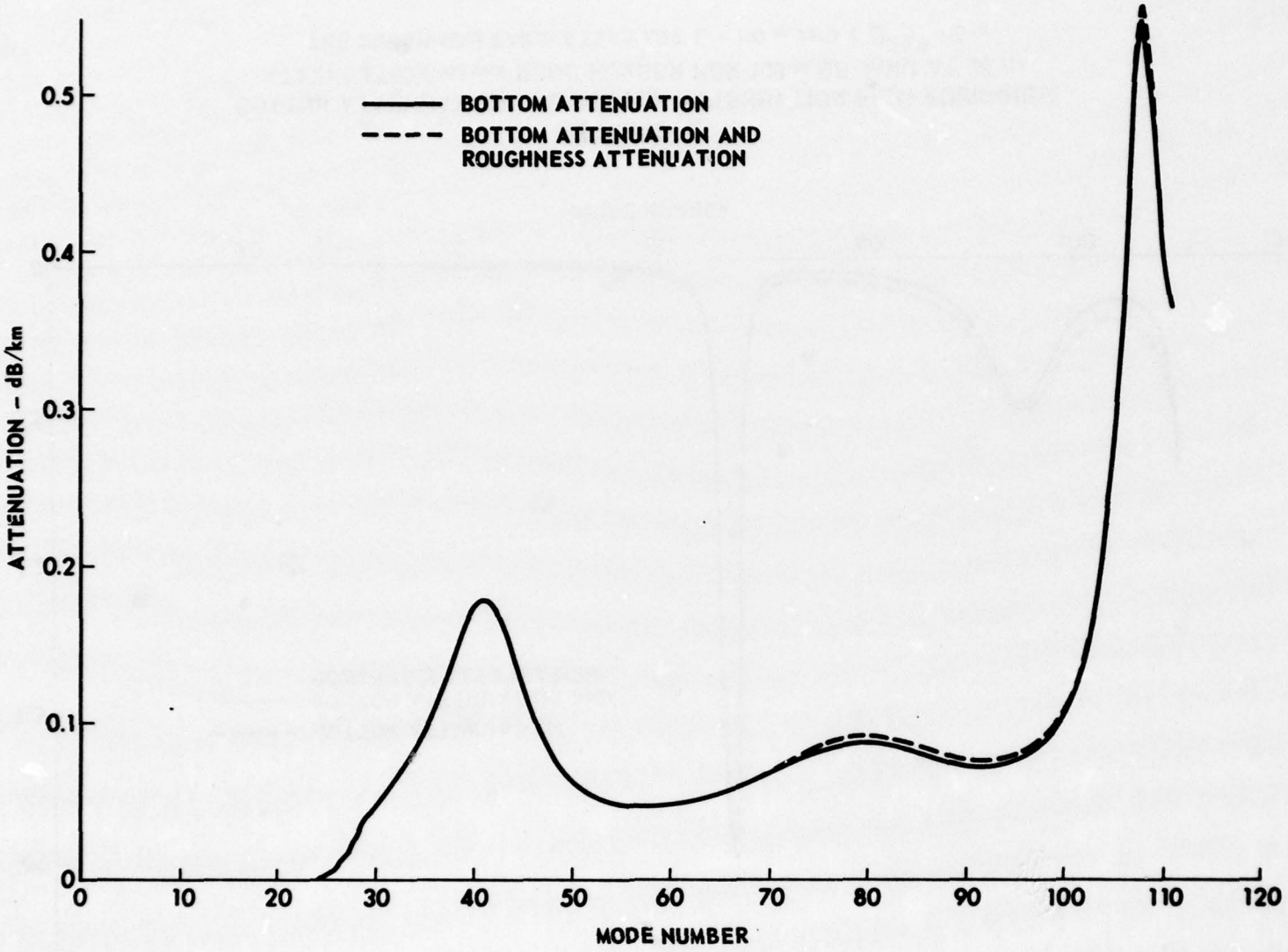

ARL:UT
AS-77-1452
SRR-GA
12-22-77

FIGURE 1
BOTTOM ATTENUATION AND BOTTOM ATTENUATION PLUS ROUGHNESS ATTENUATION versus MODE NUMBER FOR 100 m OF CLAY AT 20 Hz
THE ROUGHNESS PARAMETERS ARE L = 200 m AND $\langle \beta^2 \rangle^{1/2}$ = 5 m

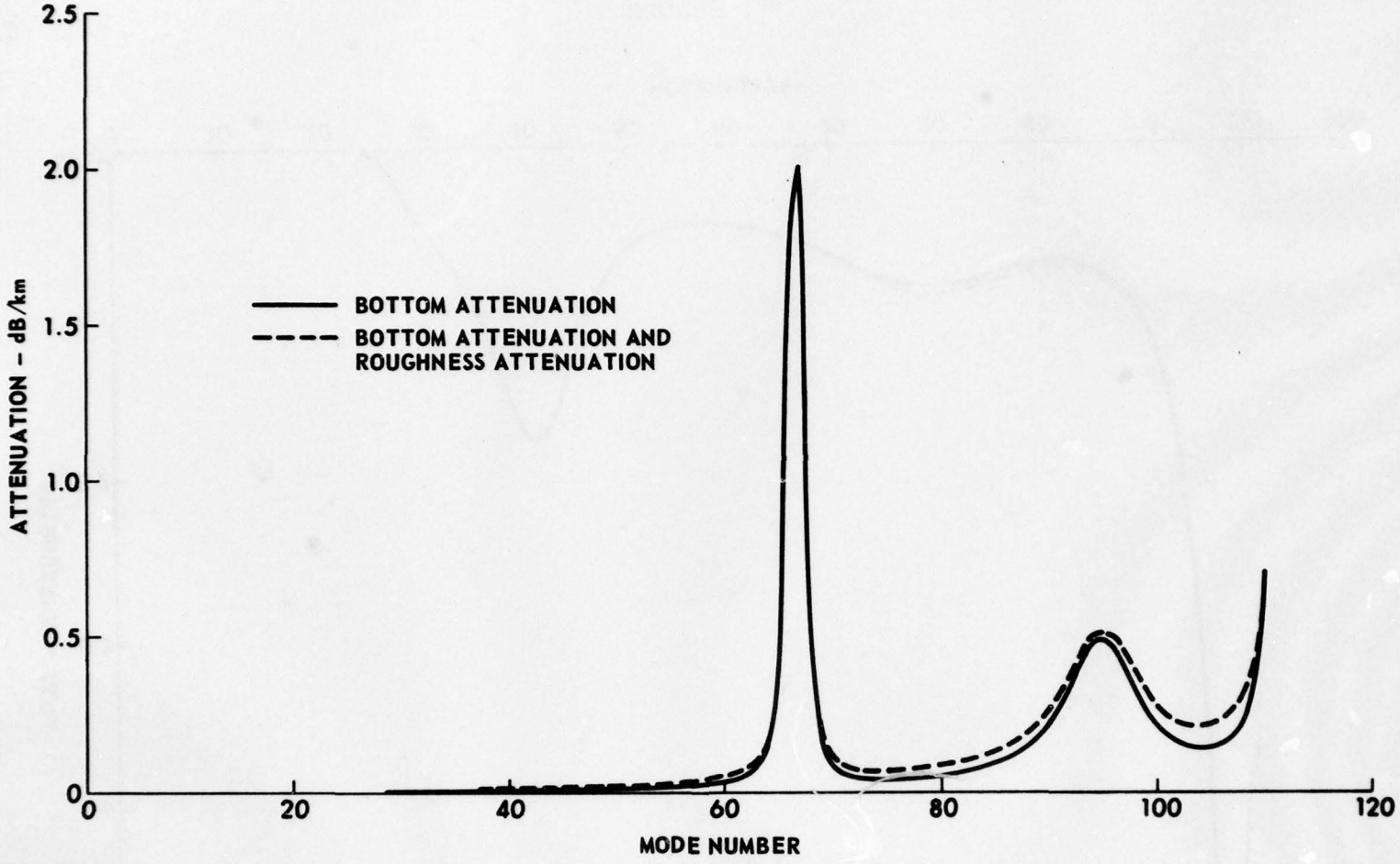

FIGURE 2

BOTTOM ATTENUATION AND BOTTOM ATTENUATION PLUS ROUGHNESS ATTENUATION versus MODE NUMBER FOR 100 m OF SAND AT 20 Hz

THE ROUGHNESS PARAMETERS ARE L = 100 m AND $\langle \beta^2 \rangle^{1/2}$ = 5 m

ARL:UT
AS-77-1457
SRR-GA
12-22-77

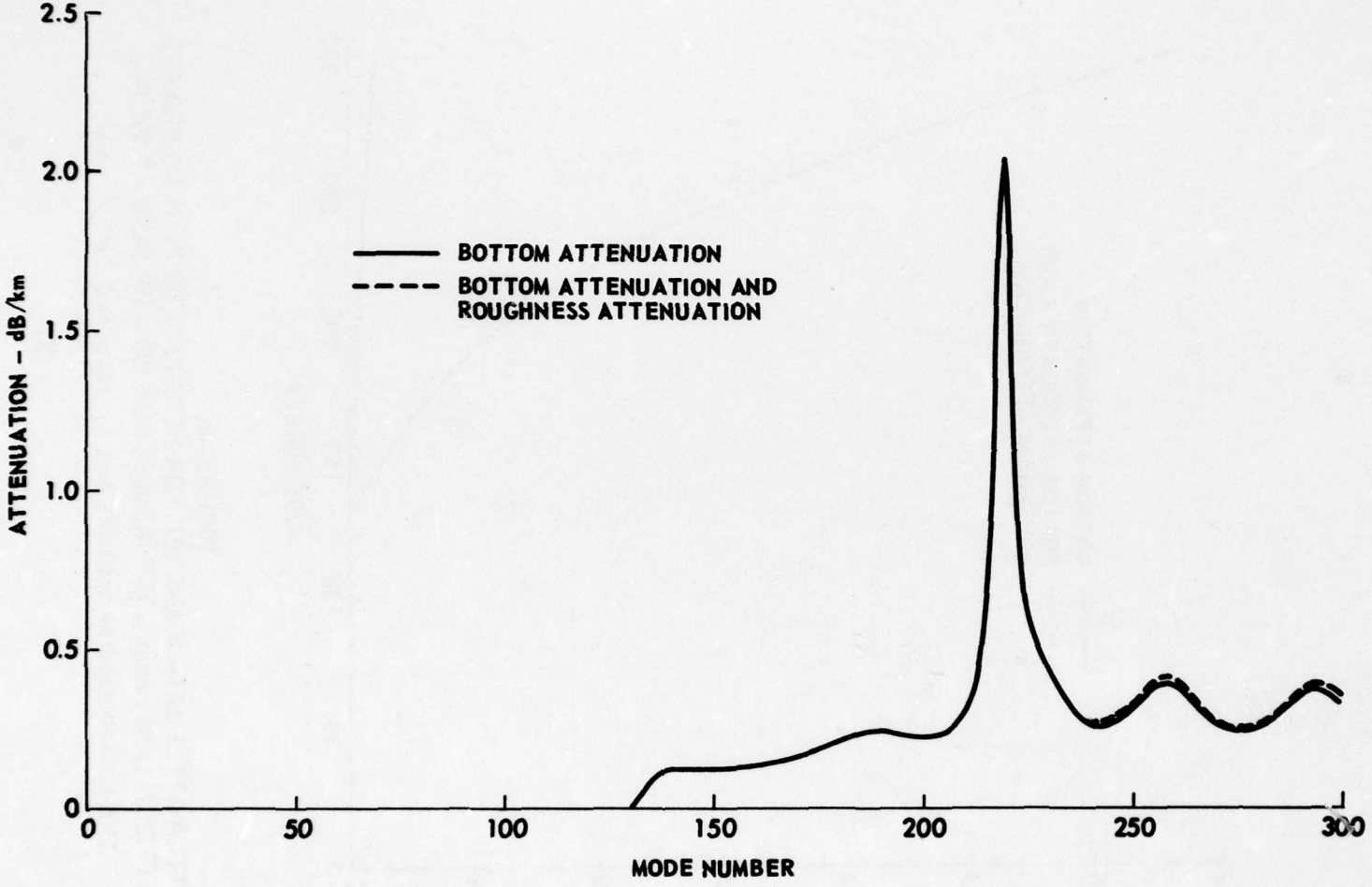

FIGURE 3
BOTTOM ATTENUATION AND BOTTOM ATTENUATION PLUS ROUGHNESS ATTENUATION versus MODE NUMBER FOR 100 m OF CLAY AT 100 Hz
THE ROUGHNESS PARAMETERS ARE L = 100 m AND $\langle \beta^2 \rangle^{1/2}$ = 5 m

ARL:UT
AS-77-1454
SRR-GA
12-22-77

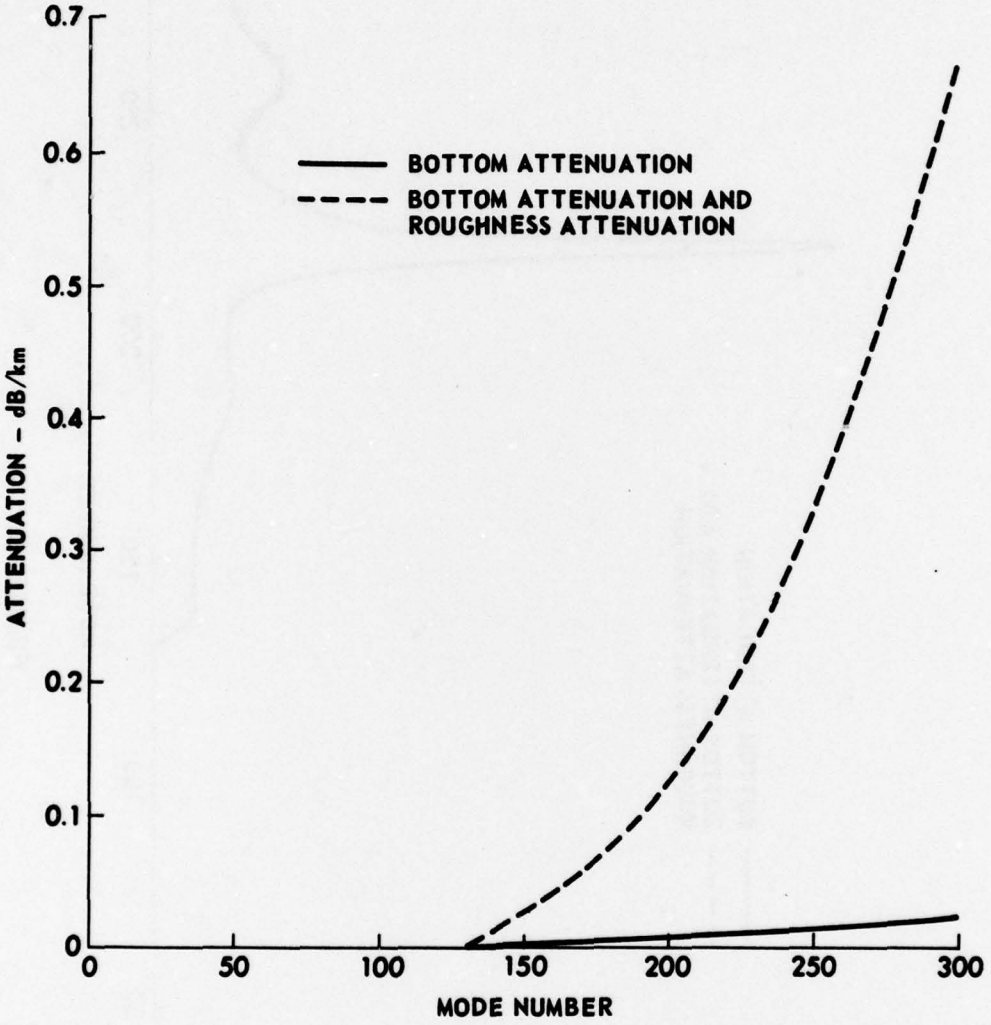

FIGURE 4
BOTTOM ATTENUATION AND BOTTOM ATTENUATION PLUS ROUGHNESS ATTENUATION versus MODE NUMBER FOR 100 m OF SAND AT 100 Hz
THE ROUGHNESS PARAMETERS ARE L = 100 m AND $\langle \beta^2 \rangle^{1/2}$ = 5 m

ARL:UT
AS-77-1459
SRR-GA
12-22-77

The question of sensitivity of these predictions to uncertainties in input roughness parameters is particularly important regarding the correlation length, L, of the roughness. This parameter, to say nothing of the correlation function which appears in the basic theory, is one which will seldom be known even approximately. Thus sensitivity of predicted values to uncertainties in L would imply that this theory would have only a limited usefulness for Navy applications. Figures 5 and 6 show δ_n^s versus mode number for two values of L. It will be observed that the predicted values of mode attenuation are quite insensitive to changes in L, even in the 100 Hz, sand sediment case where the roughness effects dominate the mode attenuation. It appears, then, that this approach has the attractive feature of being insensitive to correlation length while still retaining the advantages of treating roughness effects directly within normal mode propagation theory, with no appeal being made to either ray theory or to rough surface scattering theory.

Finally, to gain some intuition of the effects of changes in mode attenuation on propagation loss, we show the results of computations at 20 Hz for clay and sand sediments. Figures 7 and 8 show incoherent, or random phase, propagation loss versus range for a 10 m source, with and without roughness effects. The sound speed profile used in these examples was a typical mid-Pacific type with an axis at 700 m and the bottom at approximately 4900 m. As would be anticipated on the basis of the results shown in Fig. 1, roughness has very little effect for a clay bottom. In the sand bottom case the roughness is seen to cause up to a 2.5 dB increase in propagation loss. The effect of roughness, for this source-receiver geometry, begins to saturate beyond 150 km where essentially all of the bottom interacting energy has been stripped out.

B. Propagation Effects of Bottom Interaction

A line of investigation which has been an important element of this research program concerns the effects of bottom interaction on the

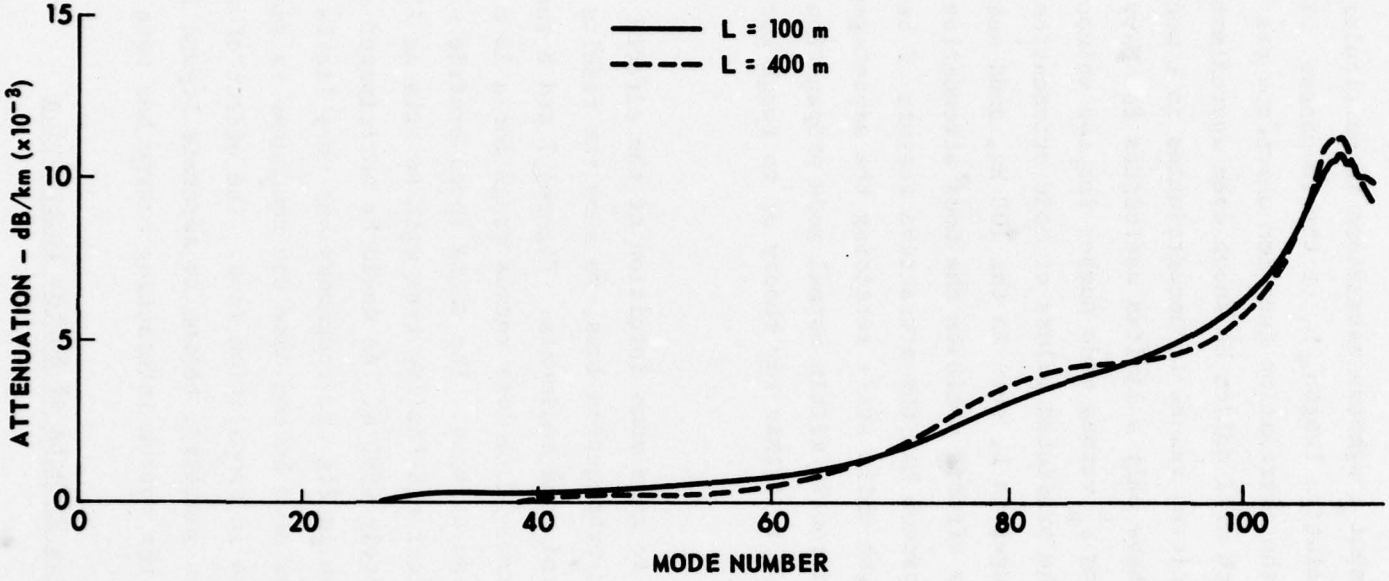

FIGURE 5
ROUGHNESS ATTENUATION versus MODE NUMBER FOR 100 m OF CLAY AT 20 Hz FOR CORRELATION LENGTHS OF 100 AND 400 m AND $\langle \beta^2 \rangle^{1/2} = 5$ m

ARL:UT
AS-77-1453
SRR-GA
12-22-77

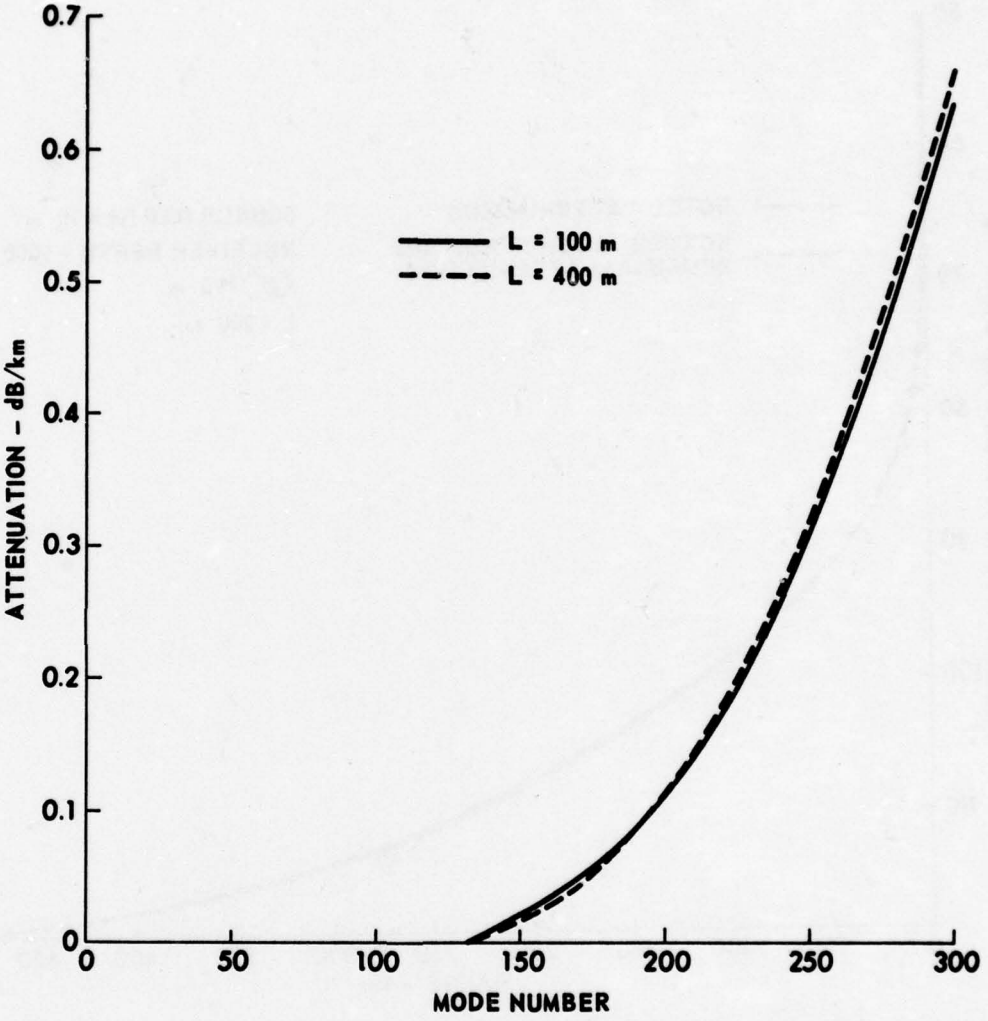

FIGURE 6
ROUGHNESS ATTENUATION versus MODE NUMBER FOR 100 m OF SAND AT 100 Hz FOR CORRELATION LENGTHS OF 100 AND 400 m AND $\langle \beta^2 \rangle^{1/2} = 5$ m

ARL:UT
AS-77-1460
SRR-GA
12-22-77

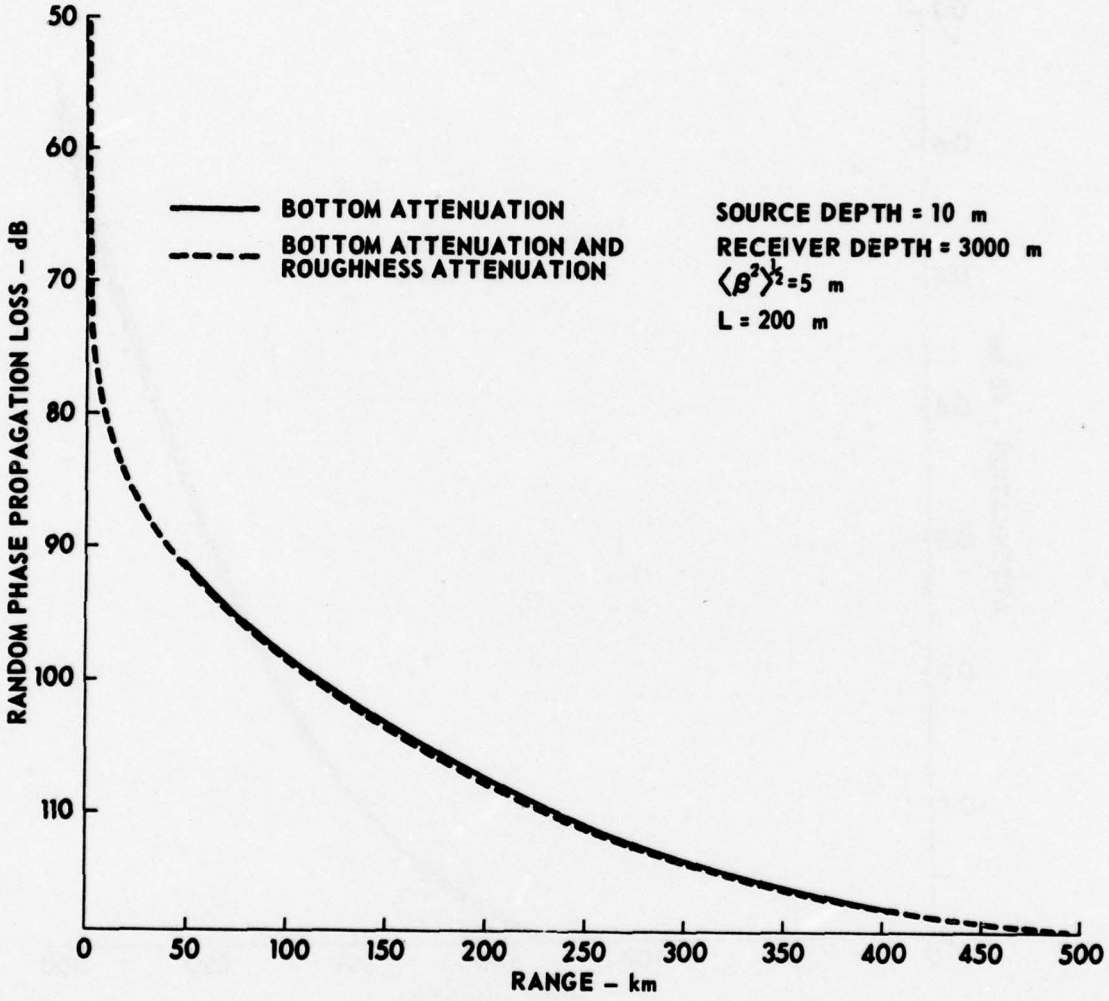

FIGURE 7
RANDOM PHASE PROPAGATION LOSS versus RANGE
FOR 100 m OF CLAY AT 20 Hz

ARL:UT
AS-78-370
SRR - GA
2 - 14 - 78

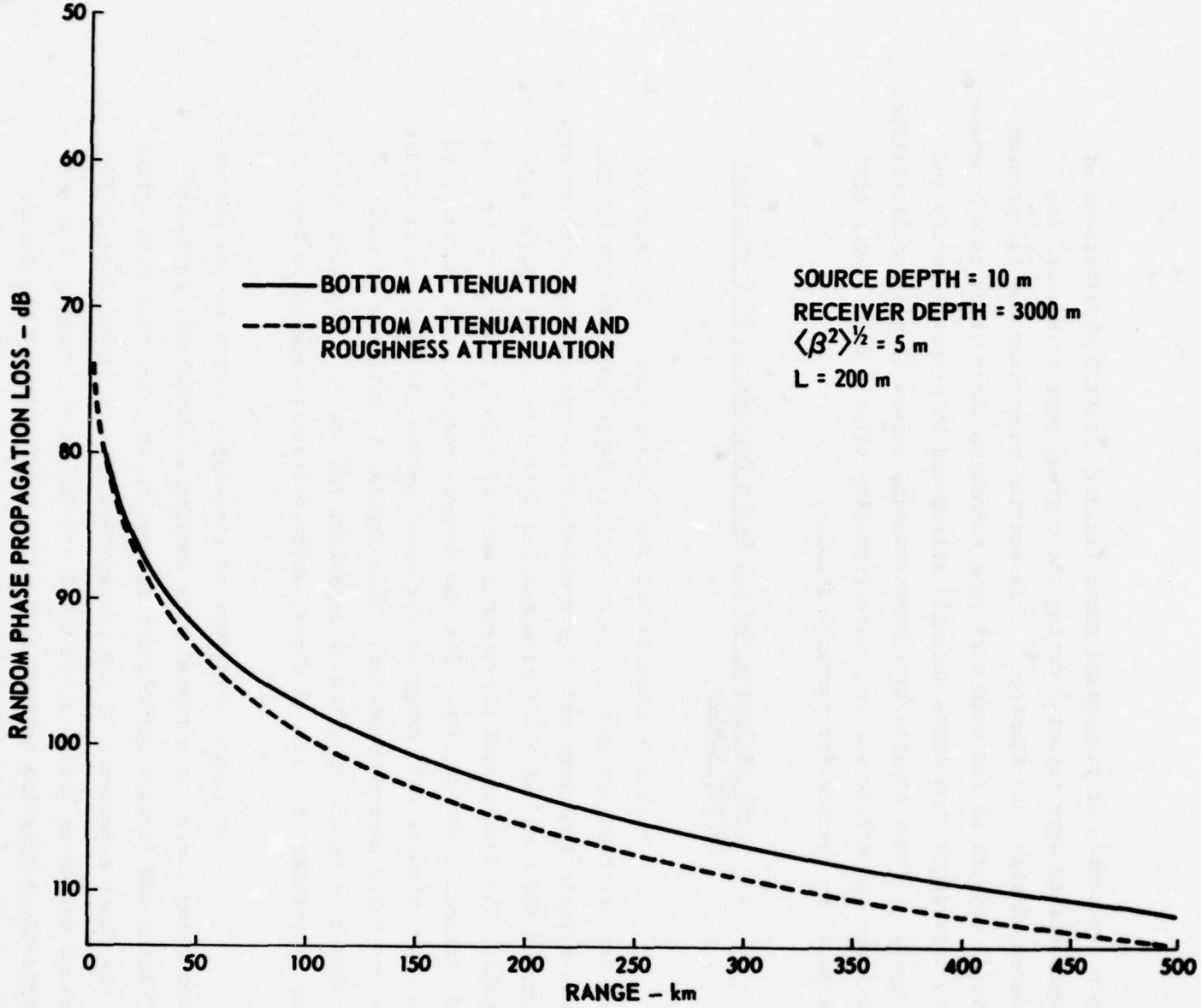

FIGURE 8
RANDOM PHASE PROPAGATION LOSS versus RANGE
FOR 100 m OF SAND AT 20 Hz

ARL:UT
AS-78-371
SRR - GA
2 - 14 - 78

depth dependence of propagated sound fields. Several applications of these studies were repeated during the current year by Hawker[3] and Shooter, Hawker, and Hampton.[4] This section summarizes and illustrates several aspects of the mode stripping mechanism which leads to a propagation loss depth dependence strongly influenced by sensor geometry and frequency. These studies have been extended beyond simple omnidirectional receivers to include vertical directionality effects illustrated here primarily by results for vertical dipoles.

1. Mode Stripping and The Depth Dependence of Propagated Sound Fields

Figure 9 shows normal mode computation of propagation loss for two receiver depths, near critical depth and near the bottom. These calculations were made for a mid-Pacific type profile with an axis depth of 700 m and with a bottom modeled as 100 m of clay overlying basalt. The anticipated convergence zone structure is clearly seen in the critical depth results. For the deeper receiver, the character of the curve changes with range as the short period oscillations disappear and the curve becomes smoother. This process is evidence of mode stripping, a mechanism which is important for the deep receiver but of less importance at critical depth, where waterborne energy is important.

As range increases, an increasing amount of the bottom interacting energy is stripped out, leaving predominantly refracted-refracted and surface reflected-refracted modes. The resulting effect on the depth dependence of the propagation loss is illustrated in Fig. 10. Various values of bottom attenuation are displayed, ranging from zero (perfectly reflecting bottom) to a value greater than a physically reasonable one for the clay sediment used in these calculations. The near-bottom gradient in propagation loss is seen to increase with both attenuation and range. Bottom interaction effects on mode stripping and the resulting effects on the depth dependence of propagated fields have been discussed by Hawker[3] and by Gordon.[5]

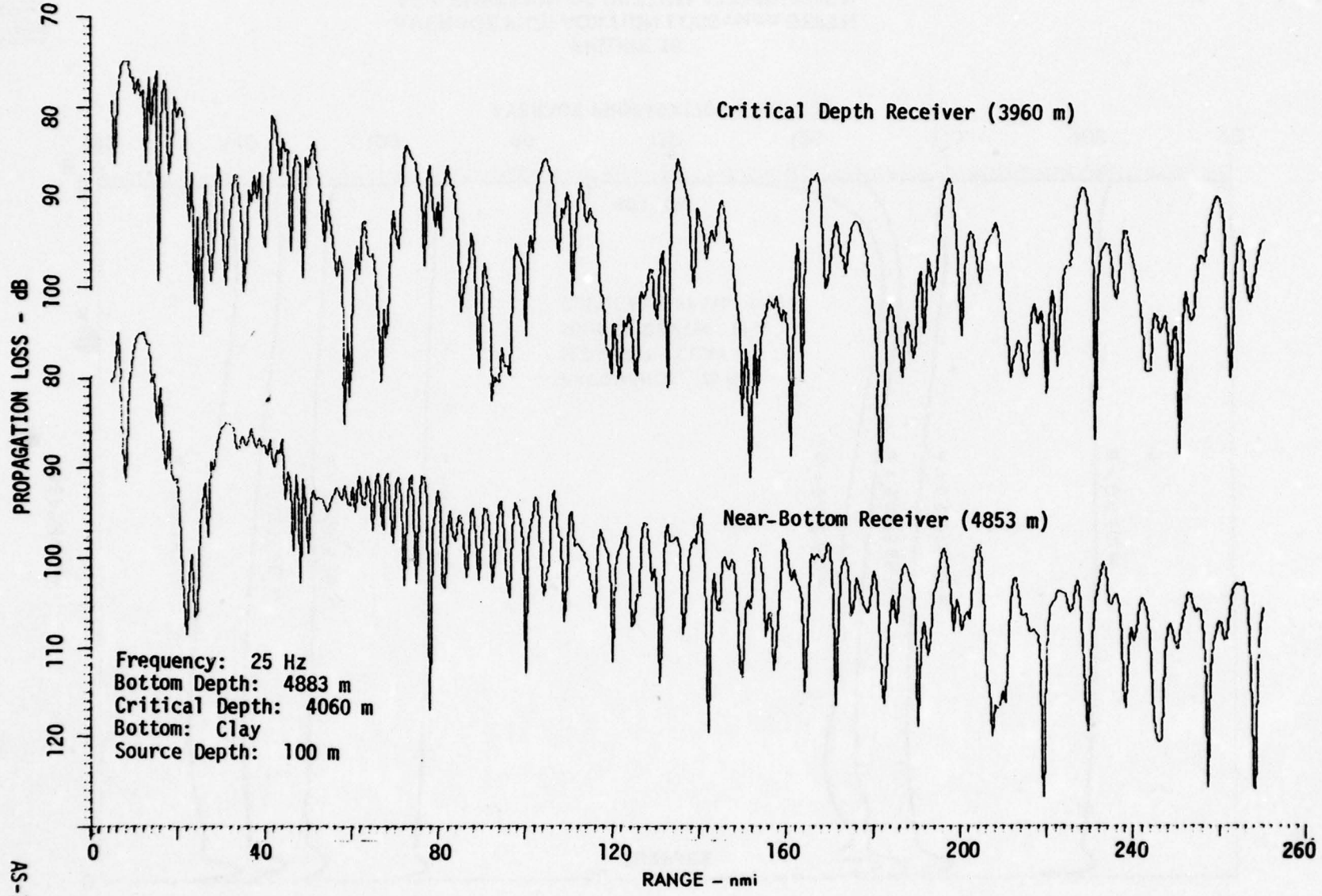

FIGURE 9
PROPAGATION LOSS versus RANGE FOR TWO RECEIVER DEPTHS ILLUSTRATING MODE STRIPPING

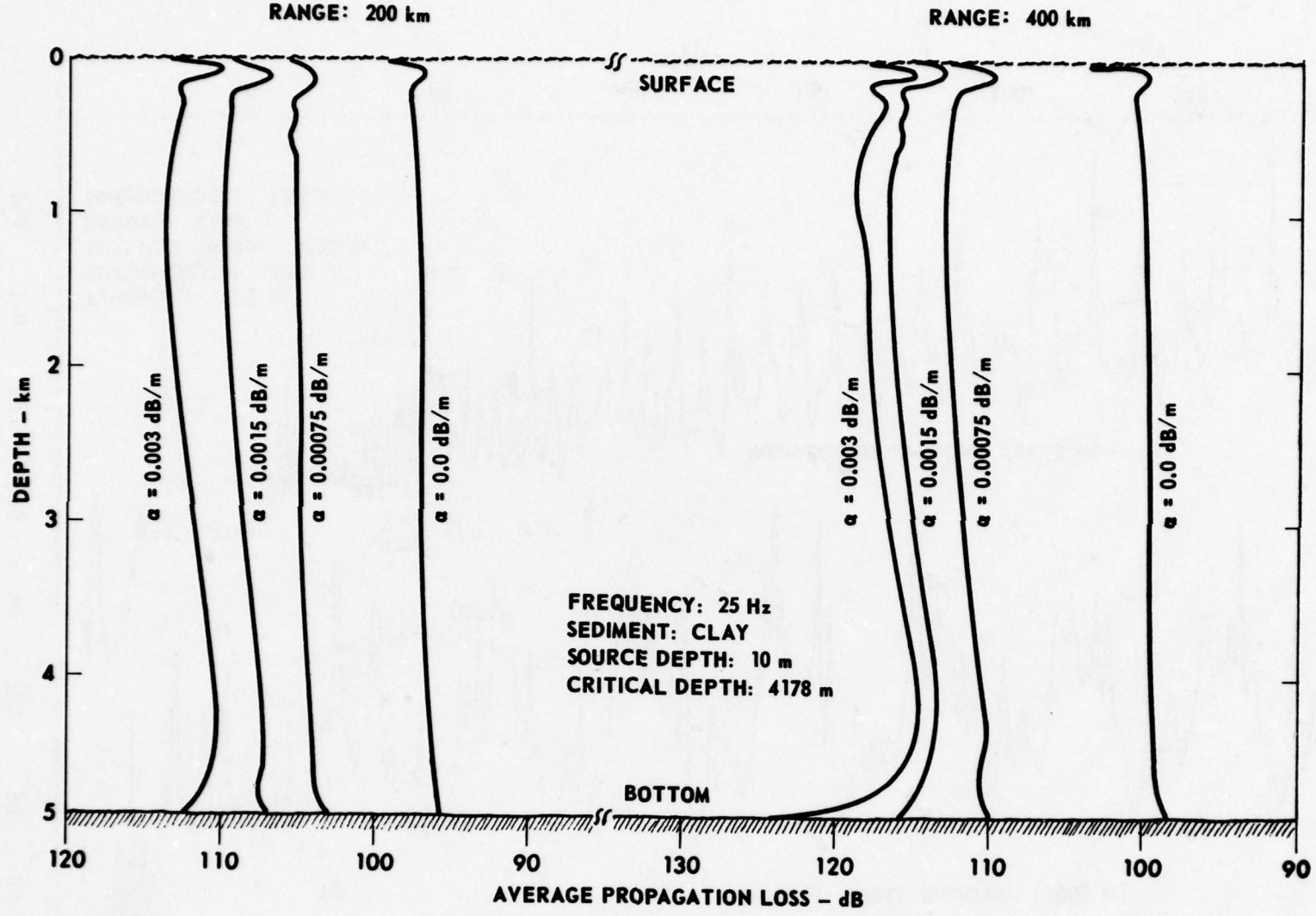

FIGURE 10
AVERAGE PROPAGATION LOSS versus DEPTH AS A FUNCTION OF BOTTOM ATTENUATION

ARL-UT-AS-77-212
KEH-DR
3-15-77

The frequency dependence of a sound pressure level versus depth curve can be quite complex with bottom absorption, surface decoupling, scattering, and duct leakage all having strong frequency dependencies. The most universal and important of the various frequency dependent mechanisms affecting depth dependence are bottom absorption and surface decoupling. Bottom absorption is thought to obey a first power law with frequency (see Hamilton[6]). The mode attenuation coefficient itself, δ_n, will have, in addition, a frequency dependence due to the duct leakage processes which appear naturally in a normal mode treatment. Surface decoupling is more complex regarding frequency dependence, but basically it arises because the pressure vanishes at the sea surface and goes to zero smoothly over a depth of several sound wavelengths of the surface.

Figures 11 through 14 show four cases, each containing three frequencies 5, 50, and 150 Hz for the source depths and ranges listed below.

	Source Depth (m)	Range (km)
Figure 11	10	20
Figure 12	100	20
Figure 13	10	200
Figure 14	100	200

These computations were carried out using a mid-Pacific type sound speed profile, having a SOFAR axis at 700 m and a clay bottom at 4883 m. The propagation loss curves are shown extended into the sediments to a depth of 5000 m. These four curves display a frequency dependence which results from a competition between surface decoupling, which tends to decrease propagation loss with increasing frequency, and bottom absorption, which tends to increase it. The basic results and dominant mechanism are listed below.

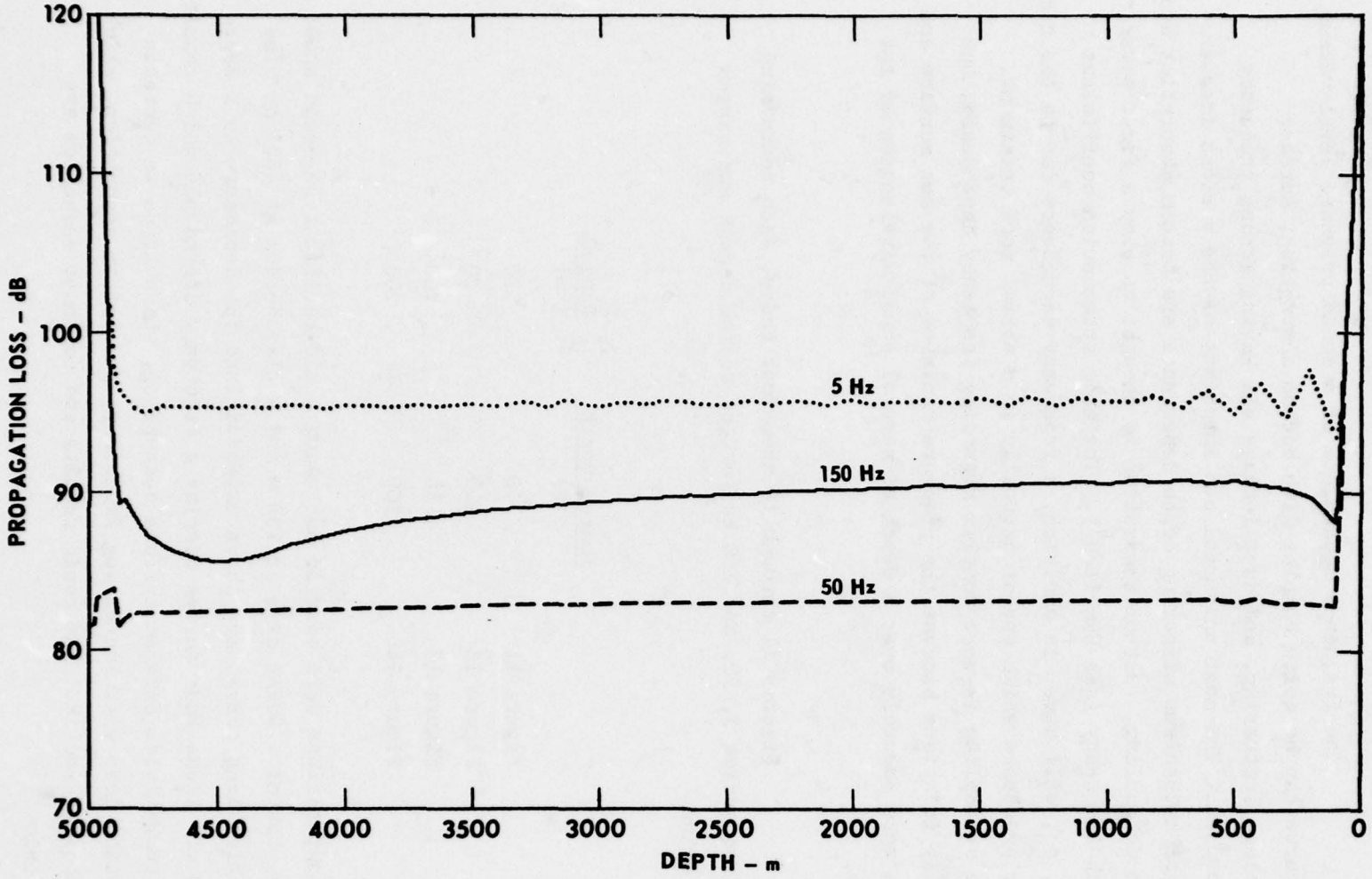

ARL:UT
AS-78-1586
KEH-GA
9-29-78

FIGURE 11
AVERAGE PROPAGATION LOSS versus DEPTH FOR A 10 m SOURCE AT 20 km RANGE

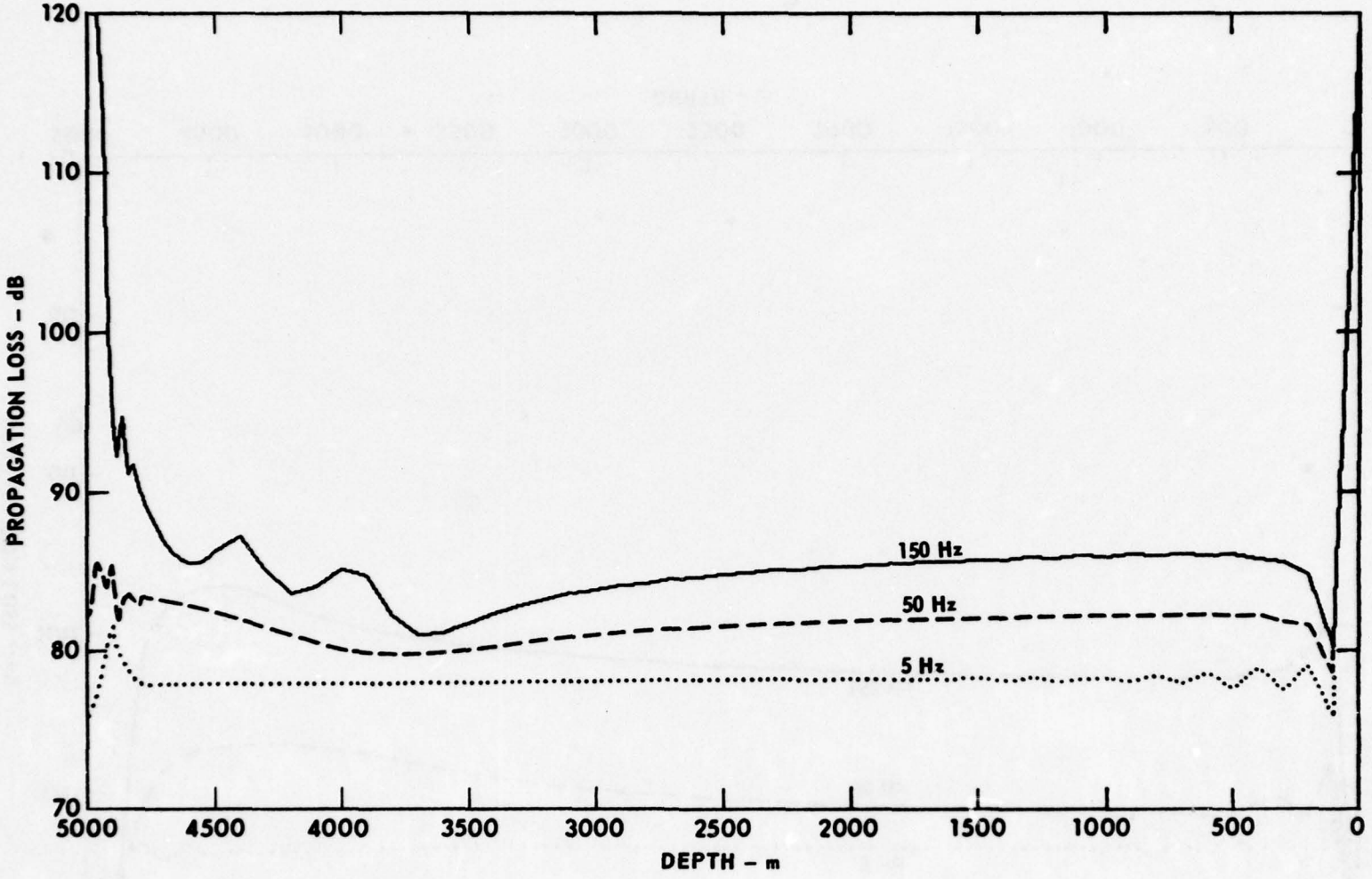

ARL:UT
AS-78-1585
KEH-GA
9-29-78

FIGURE 12
AVERAGE PROPAGATION LOSS versus DEPTH FOR A 100 m SOURCE AT 20 km RANGE

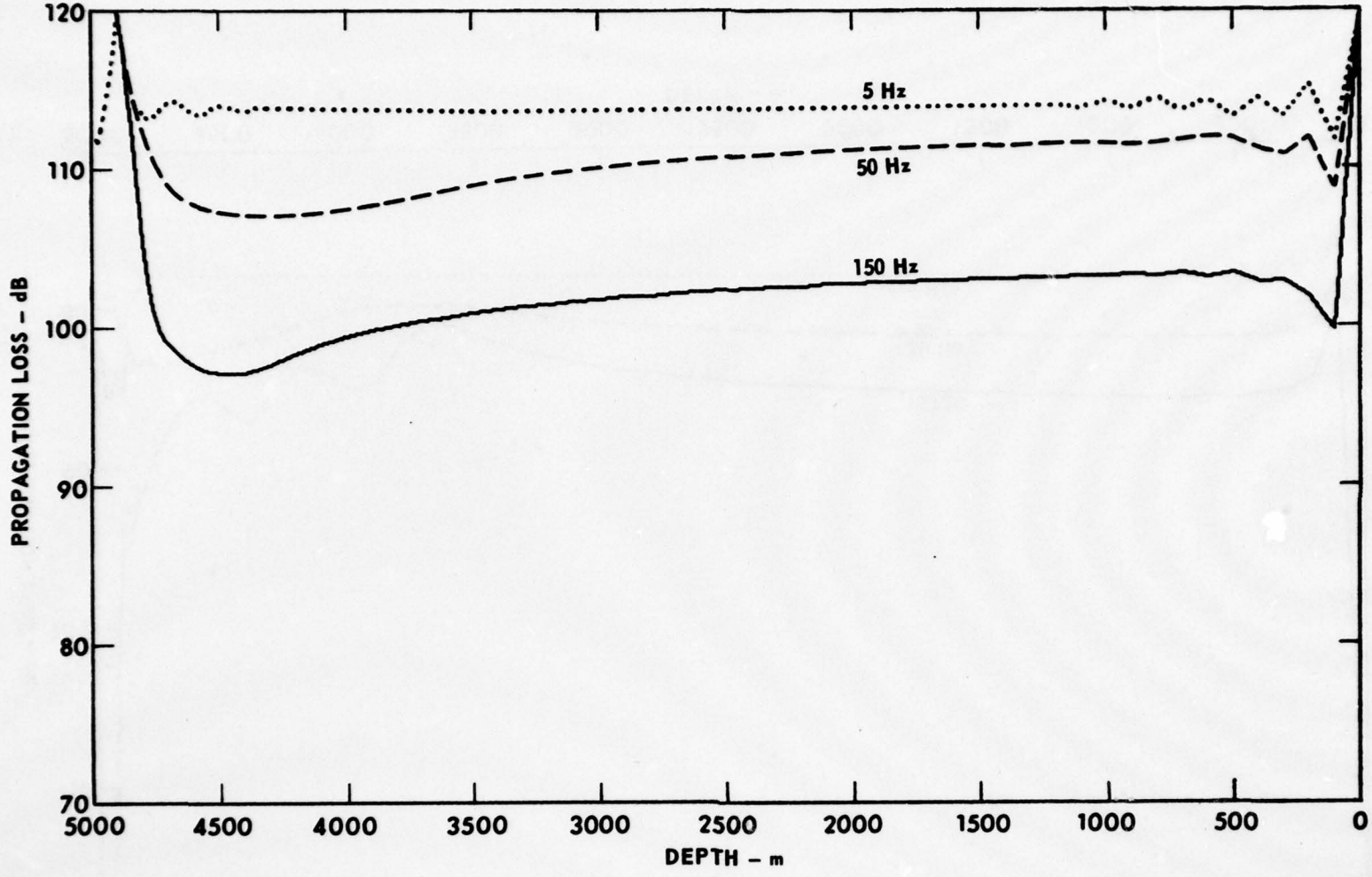

ARL:UT
AS-78-1587
KEH-GA
9-29-78

FIGURE 13
AVERAGE PROPAGATION LOSS versus DEPTH FOR A 10 m SOURCE AT 200 km RANGE

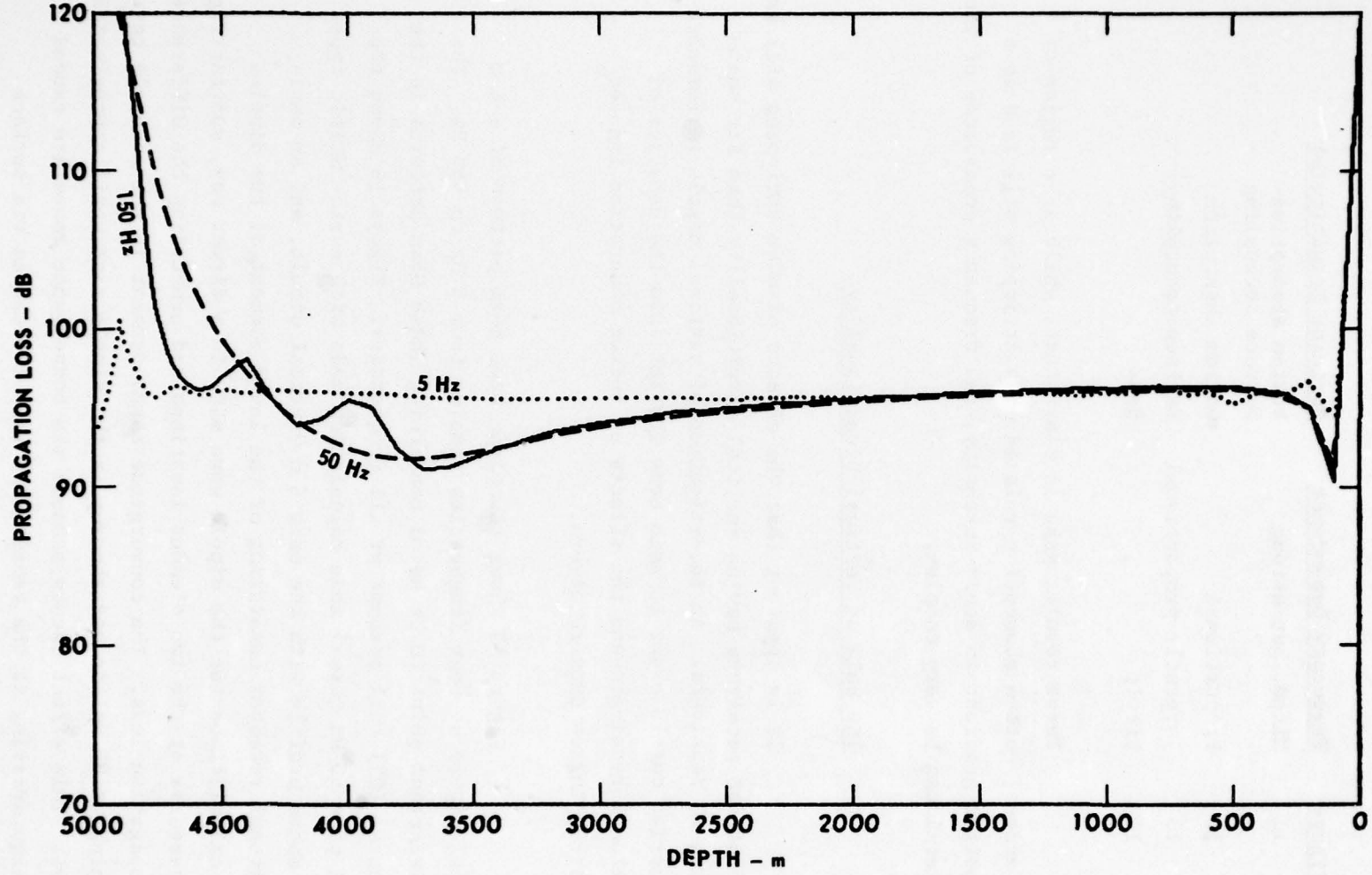

ARL:UT
AS-78-1619
KEH-GA
10-16-78

FIGURE 14
AVERAGE PROPAGATION LOSS versus DEPTH FOR A 100 m SOURCE AT 200 km RANGE

Figure	Frequency Dependence	Dominant Mechanism(s)
11	Mixed, but strong	Bottom absorption Surface decoupling
12	Proportional	Bottom absorption
13	Inversely proportional	Surface decoupling
14	Little	None

These results make it clear that, while in a region of depth excess, bottom absorption related mode stripping will lead to a near-bottom gradient in sound intensity; the frequency dependence of the mean level can be very complex.

2. The Role of Vertical Directionality

It is apparent that the effects of mode stripping will be different for receivers having vertical directionality than for omni-directional receivers. An investigation of vertical dipole performance was carried out in order to gain some insight into the behavior of directional receivers and the effects of bottom absorption induced mode stripping on such receivers.

Figure 15 shows the plane wave beam pattern of a 6 m vertical dipole at four frequencies ranging from 5 Hz to 150 Hz. The most important point to be noted concerning these beam patterns is the horizontal (0°) null present at all frequencies. Figure 16 shows the result of a 50 Hz normal mode calculation made with a mid-Pacific type sound speed profile with the same 6 m vertical dipole, and an omni-directional receiver consisting of the lower element of the dipole. These calculations for the dipole were made in a direct way, subtracting the pressures at the two element locations and converting the difference to propagation loss. The convergence zones present in the monopole case beginning at 80 nmi do not show up in the dipole case until approximately 140 nmi. This effect occurs because the convergence zones are caused by energy arriving at the receiver at very low angles via surface reflected-bottom refracted paths, the very low angle paths most

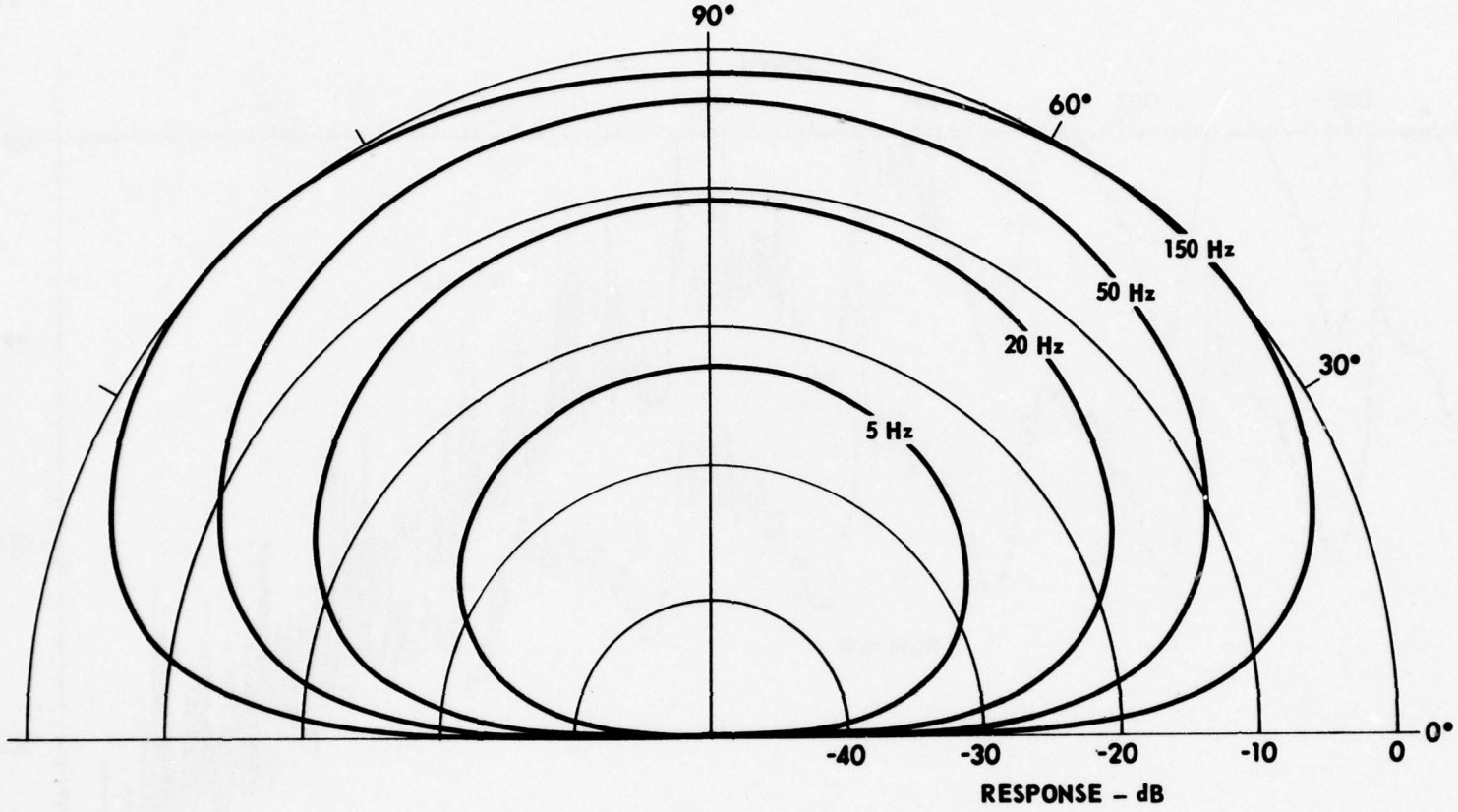

FIGURE 15
PLANE WAVE RESPONSE OF A 6 m VERTICAL DIPOLE AT FOUR FREQUENCIES

ARL - UT
AS-77-991
KEH - DR
8 - 11 - 77

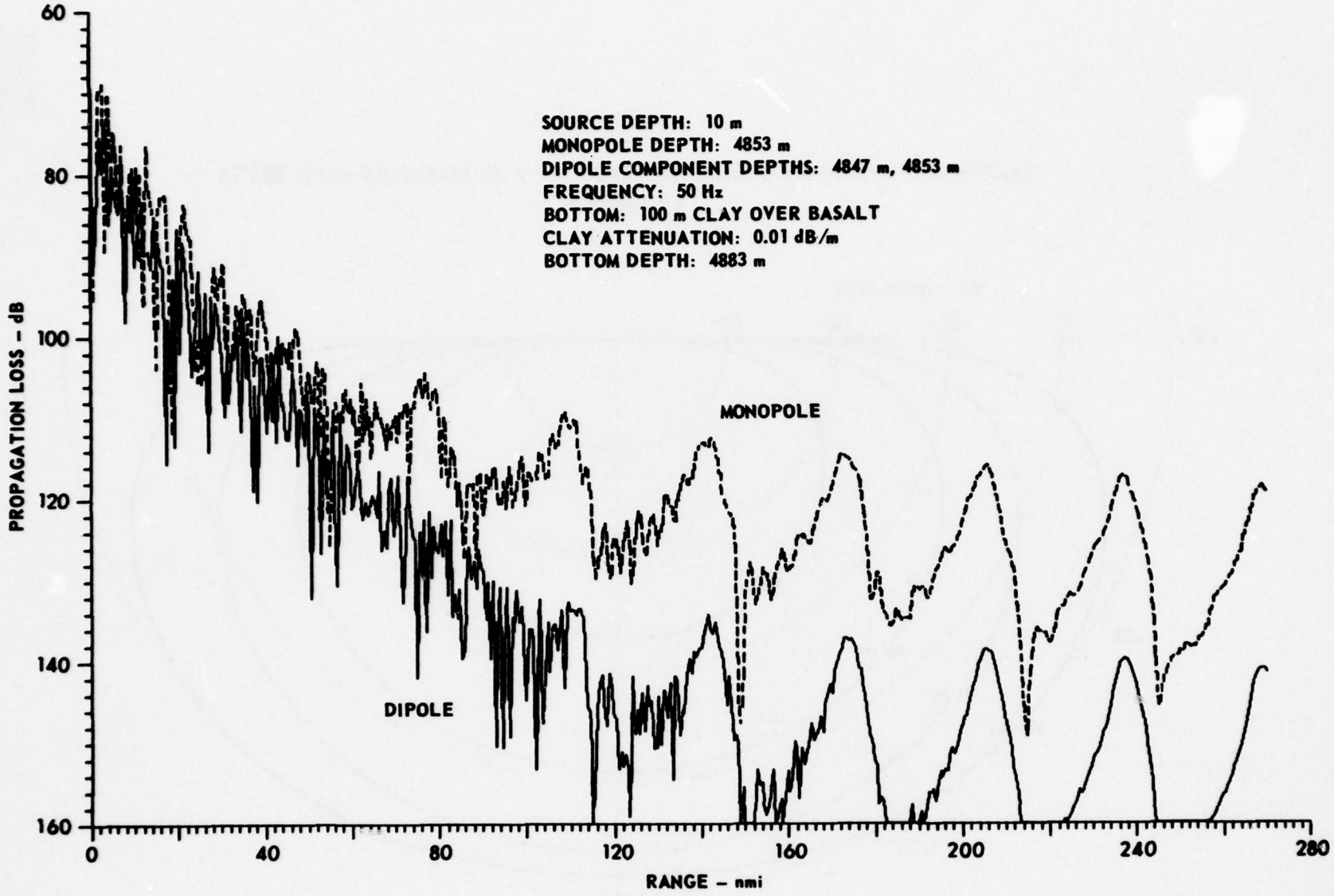

ARL - UT
AS-77-726
KEH - DR
6 - 23 - 77

FIGURE 16
PROPAGATION LOSS versus RANGE FOR MONOPOLE AND DIPOLE RECEIVERS
AT 50 Hz WITH A MID-PACIFIC TYPE PROFILE

discriminated against by the dipole. Thus more high angle bottom interacting energy must be stripped out in order for the convergence zones to be seen.

Figures 17 through 19 show the differences in propagation loss between the monopole and dipole, called dipole rejection here and signal gain in other works, for three frequencies. In each figure bottom absorption is given for upper and lower bounds of physically reasonable values for the clay sediment used in the model.

In Fig. 17, at 50 Hz, as range increases the dipole rejection begins a slow decrease in the low attenuation case and a much more rapid decrease for the high attenuation case. At long ranges the two curves begin to approach each other. The behavior of these curves can be understood on the basis of mode stripping and the association of modes and rays. As range increases and mode stripping begins, the acoustic field near the bottom begins to have a large fraction of energy in low angle paths. These low angle paths, as we saw in Fig. 16, are rejected strongly by the dipole. Thus the dipole propagation loss increases more rapidly than the monopole loss, driving the dipole rejection downward. Moreover, this process is more rapid (with range) for a high loss bottom than for a low loss bottom.

At lower frequencies the dipole has reduced sensitivity at high angles (see Fig. 15). Moreover, the mode stripping process proceeds more slowly due to lower mode attenuation coefficients. The result is a decreased average dipole rejection and less sensitivity to bottom attenuation. These effects are clearly illustrated in the 5 Hz calculations of Fig. 18. As frequency is increased from 50 Hz, the increased normal incidence response of the dipole decreases the average dipole rejection, as illustrated in Fig. 19.

Although the basic character of these vertical dipole results can be obtained by combining a plane wave beam pattern with the

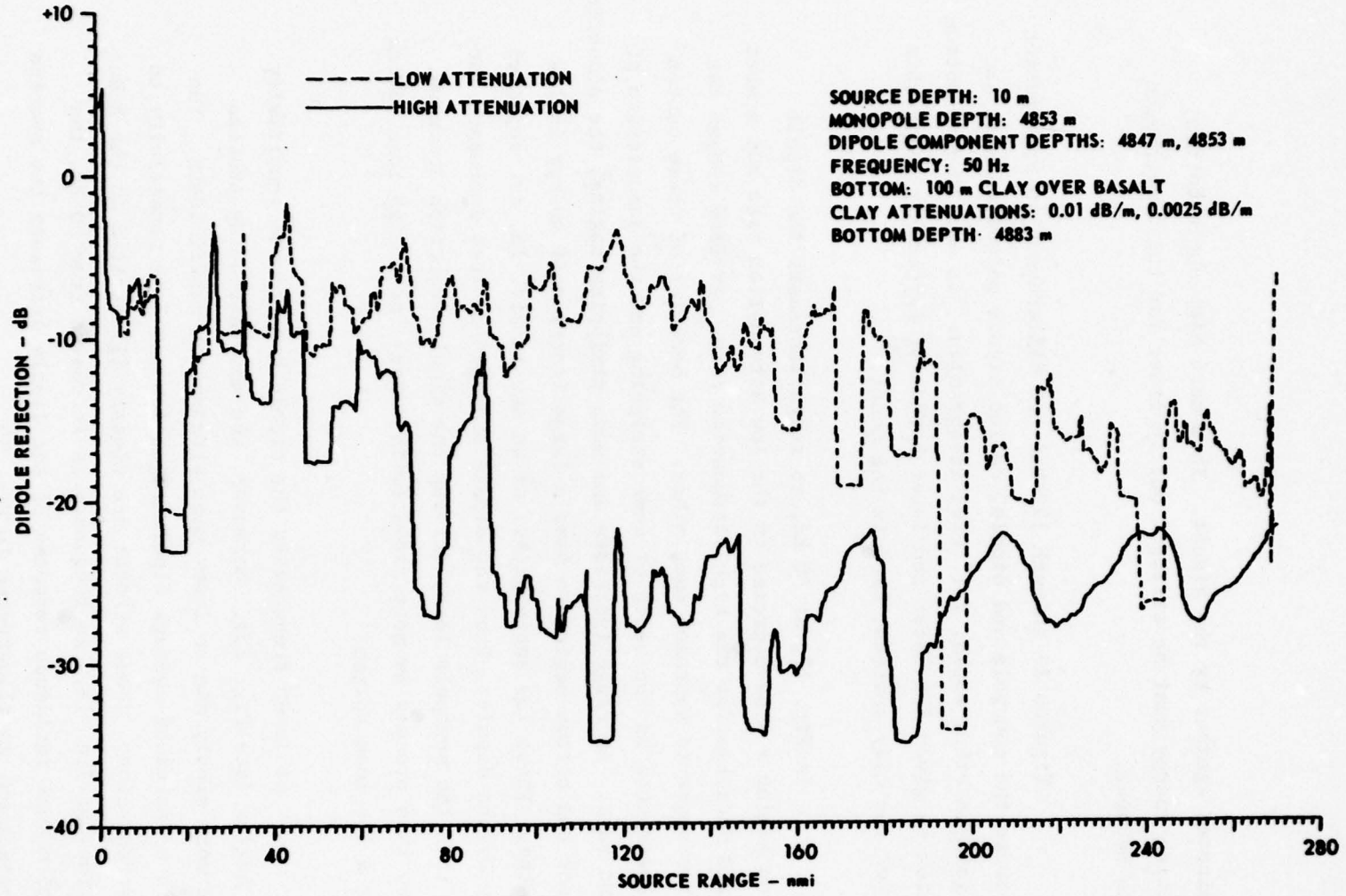

ARL - UT
AS-77-723
KEH - DR
6 - 23 - 77

FIGURE 17
DIPOLE REJECTION versus SOURCE RANGE AT 50 Hz FOR NEAR-BOTTOM RECEIVERS WITH A MID-PACIFIC TYPE PROFILE

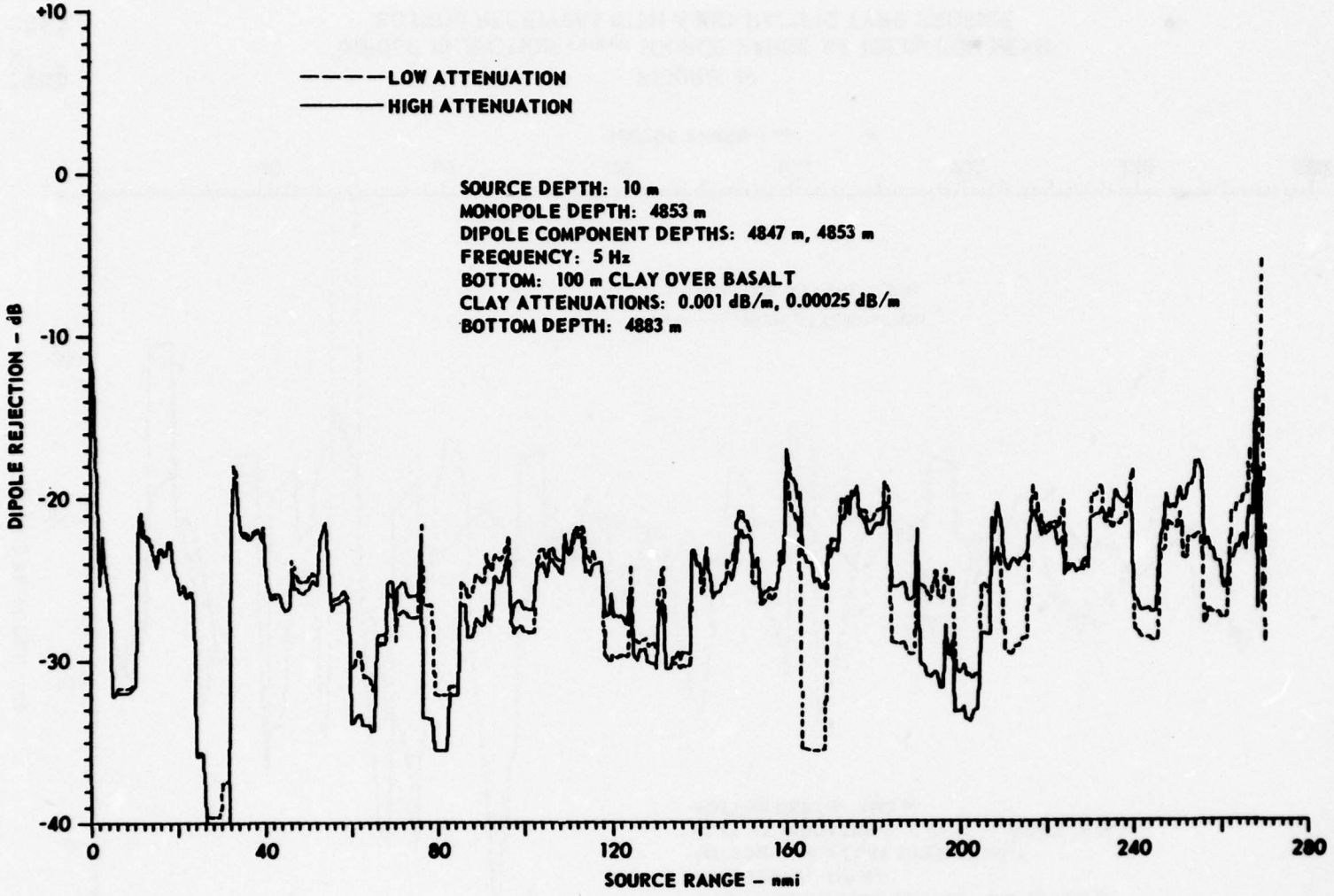

ARL - UT
AS-77-719
KEH - DR
6 - 23 - 77

FIGURE 18
DIPOLE REJECTION versus SOURCE RANGE AT 5 Hz FOR NEAR-BOTTOM RECEIVERS WITH A MID-PACIFIC TYPE PROFILE

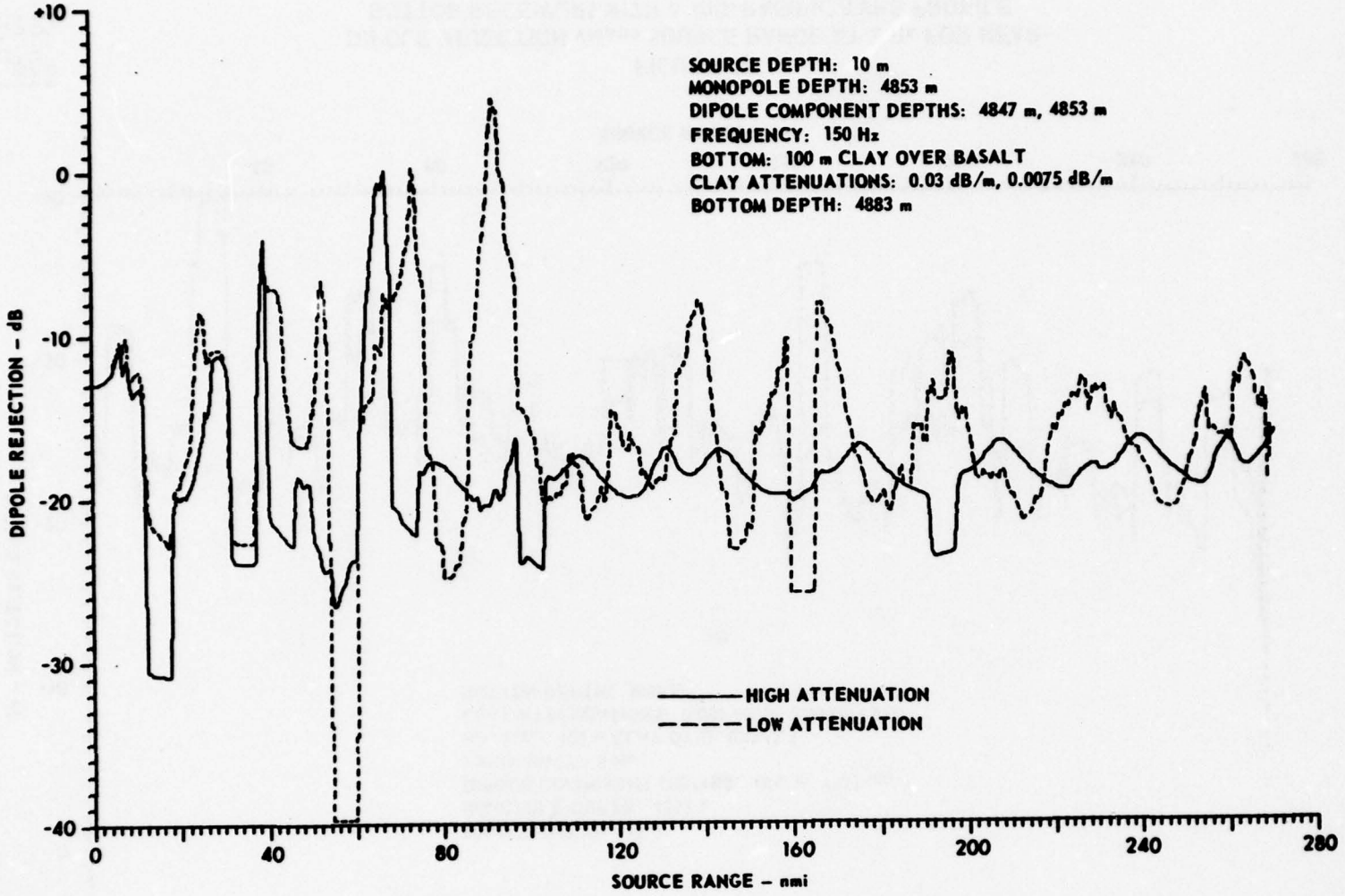

ARL - UT
AS-77-720
KEH - DR
6 - 23 - 77

FIGURE 19
DIPOLE REJECTION versus SOURCE RANGE AT 150 Hz FOR NEAR-BOTTOM RECEIVERS WITH A MID-PACIFIC TYPE PROFILE

results of a ray trace calculation to the center of the dipole, the proximity of the boundary (the bottom) renders the details of such a calculation suspect quantitatively. Not only does the amplitude of the acoustic field change rapidly near the bottom, especially in the mode stripping region, but an array, such as a dipole, is also sensitive to phase errors. The direct normal mode calculations carried out here not only are free from such ray theoretical artifacts but also properly treat bottom refracting energy as well as energy reflected from the water-sediment interface.

3. Vertical Line Arrays

During the present contract year, work was begun to extend investigation of bottom interaction effects on directional receivers beyond the vertical dipole results outlined in the previous section. In particular, a normal mode model for direct beamforming on multielement vertical line arrays was developed, and the required computer software was written and tested. This model functions by computing the complex pressure at each array element location and then constructing beams by time delay (phase shift) beamforming. The model has the capability for treating amplitude shaded, steered, nonuniformly spaced line arrays.

Figure 20 shows the sensor configuration and array element locations for a 25-element, 50 Hz array used as a test case. The lowest element in the array was located 2 m above a clay bottom having a sound speed gradient of 1.0 sec^{-1}. Figure 21 shows a three-dimensional representation of array response versus range versus steering angle, the former ranging from 6 km to 100 km and the latter from +90° (vertically upward) to -90° (vertically downward). The various arrival orders are clearly evident in the figure, with the first such order representing direct path arrivals. Because of the direct beamforming method used (having no appeal to plane wave beam patterns), these computations accurately represent the array response even though the array extends over a region where the average pressure can be expected to vary several decibels across the array aperture.

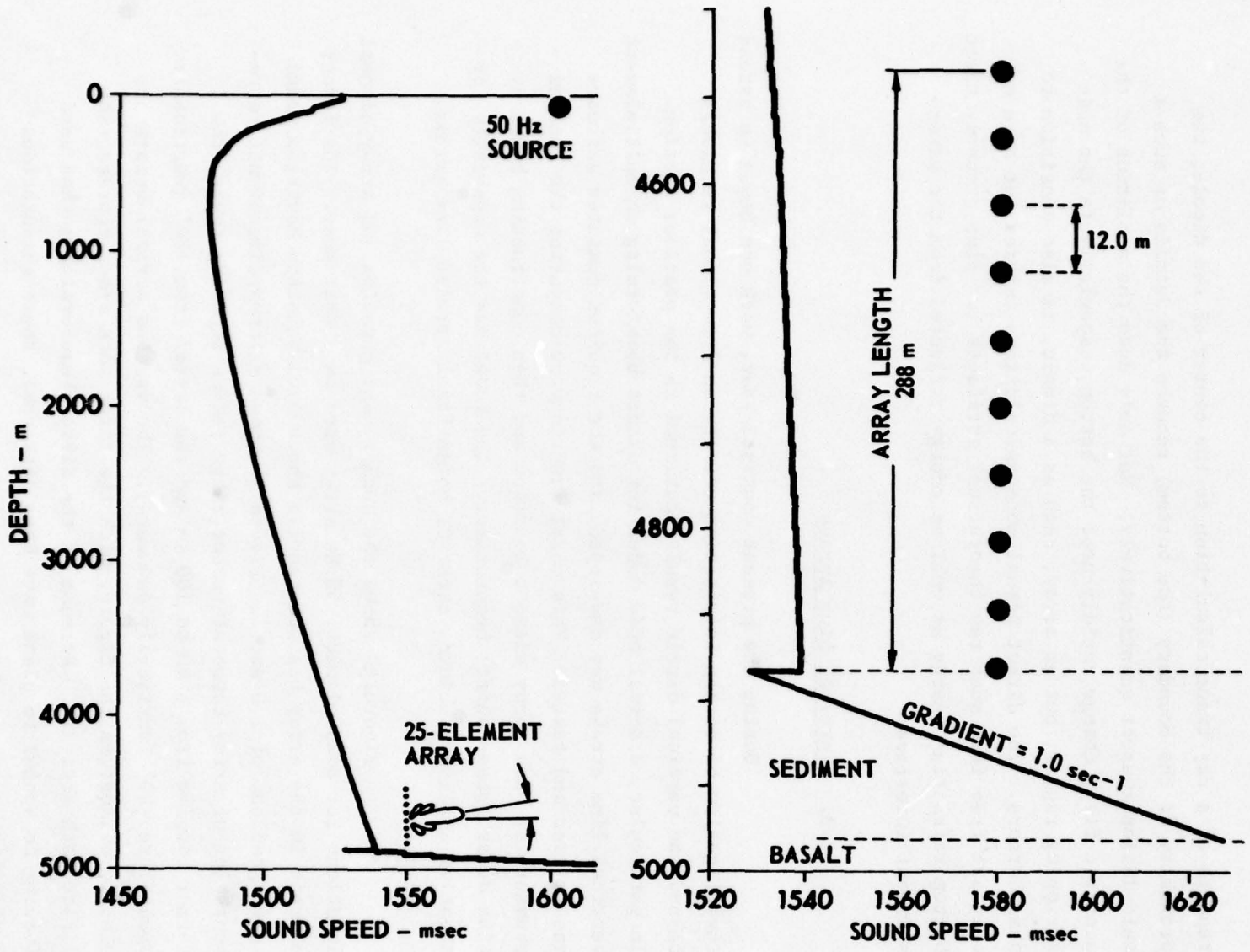

ARL - UT
AS-77-1279
KEH - GA
10 - 28 - 77

FIGURE 20
VERTICAL LINE ARRAY

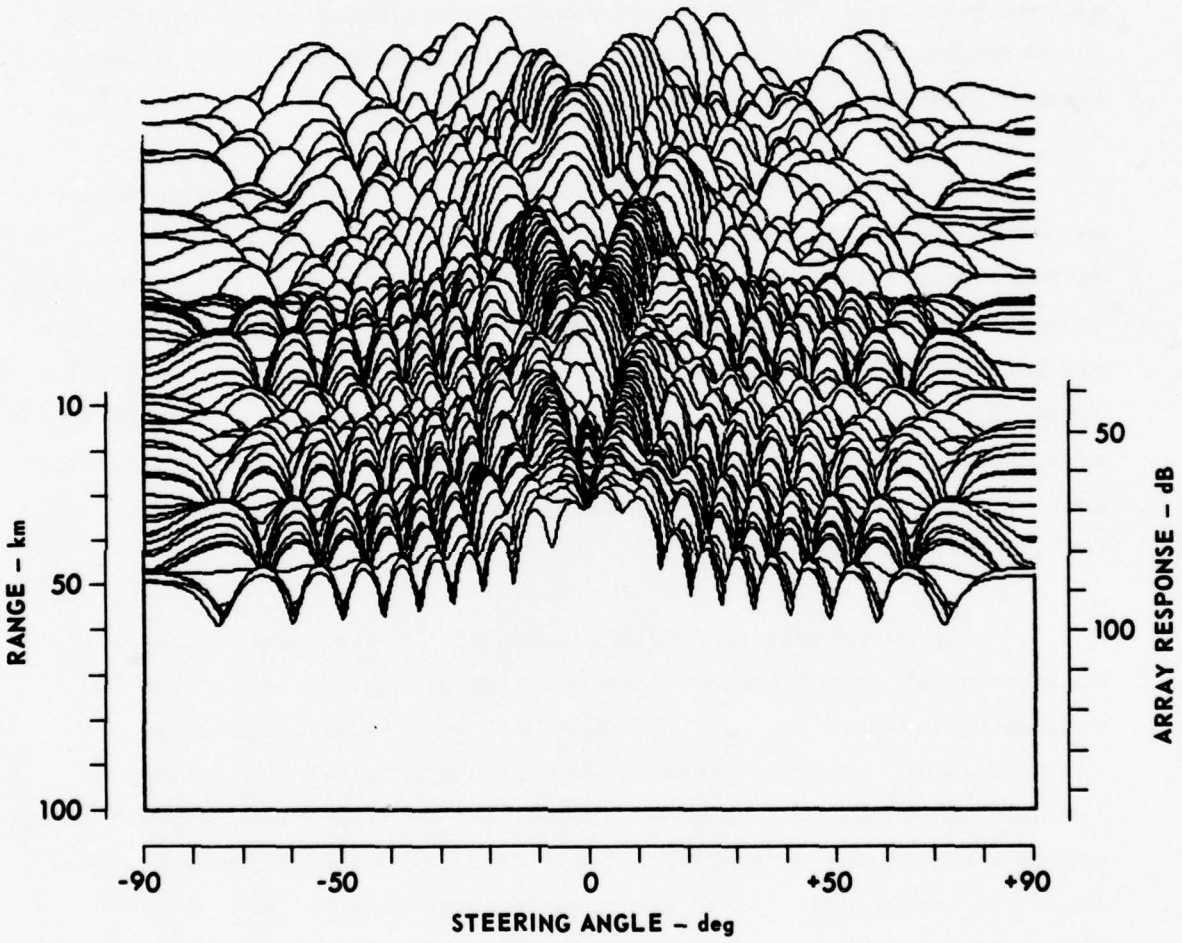

FIGURE 21
ARRAY RESPONSE versus RANGE AND STEERING ANGLE
FOR A 50 Hz, 100 m SOURCE

ARL:UT
AS-78-1632
KEH - GA
10 - 19 - 78

C. Bottom Loss Sensitivity Studies

Various bottom loss sensitivity studies have been brought to completion and documented during the present contract year. These include studies of the effects of density and attenuation gradients in the subbottom, as well as studies concerning the importance of a basalt basement underlying unconsolidated sediments.

An investigation of the effects of sediment density gradients on bottom reflection loss, begun during FY 76, was brought to completion during the present year. This work (Rutherford and Hawker[2]) showed that such gradients were essentially unimportant at low grazing angles. A possible exception to this conclusion was the small shift in the angular location of a Stoneley wave related bottom loss peak due to the presence of a density gradient. At high grazing angles, it was found that density gradients could exert a significant, though still not dominating, influence on reflection loss.

An investigation of the effects of the presence of a basalt basement on bottom reflection loss was also brought to conclusion and documented (Hawker[8,9]). It was found that a particular boundary, or interface wave, called a Stoneley wave, could exist at the sediment-basement interface and, moreover, could lead to very large ($\approx$20 dB) though narrow peaks in the bottom reflection loss. Although this effect could occur for homogeneous "fast" sediments such as sand, a case of more practical interest was the low speed soft sediment (clay) having a sound speed gradient. In such sediments, Stoneley wave effects could remain large for sediment thicknesses up to several hundred meters. Future work in this direction should include determining whether sediment rigidity (shear waves) exerts an appreciable influence on this Stoneley wave effect.

An investigation of the role of sediment attenuation gradients on bottom reflection loss was completed during the present contract year.

It was found (Hawker, Williams, and Foreman[10]) that, at low grazing angles, the presence of a strong ($\approx$1.0 sec^{-1}) sound speed gradient rendered bottom reflection loss sensitive to the surficial attenuation value but insensitive to the attenuation gradients at depth. At higher grazing angles, or in the absence of a strong sound speed gradient, bottom reflection loss could be very sensitive to the attenuation gradient. When an entire sediment layer was insonified, the variable attenuation profile was found to behave exactly as a constant attenuation value having the value of the layer average of the actual attenuation. These conclusions are illustrated in the following examples drawn from Ref. 10.

Figure 22 shows the computed bottom loss versus grazing angle for a 300 m layer of clay overlying a basalt substrate. For the moment, the clay layer is treated as having a constant sound speed, and the attenuation is treated in two ways, with the lossless case included for reference. It will be observed that, except at the lowest angles, as the loss approaches zero, the constant (surficial) attenuation profile case differs markedly from the case of a linearly increasing attenuation. By contrast, Fig. 23 shows the same situation but with the sediment assumed (somewhat more realistically) to have a sound speed linearly increasing with depth. The situation is seen to be drastically altered from that of Fig. 22 at low grazing angles. The effects of the upward refracting sound speed gradient now yield results which could be anticipated on the basis of the total ray path attenuation, as discussed in Ref. 10. In particular we see that, at low grazing angles, there is very little sensitivity to the attenuation profile. In the case considered in Fig. 23 the ray paths would first encounter the basalt at approximately 32°, leading to the general decrease in loss beyond this angle. At high grazing angles it will be seen that the effect of a linear increase in attenuation leads to substantial increases in loss with respect to the constant attenuation case.

The simple picture of attenuation effects obtained by a ray path analysis is further confirmed by the results shown in Fig. 24. For the same 300 m clay layer (over basalt) as considered in Figs. 22 and 23

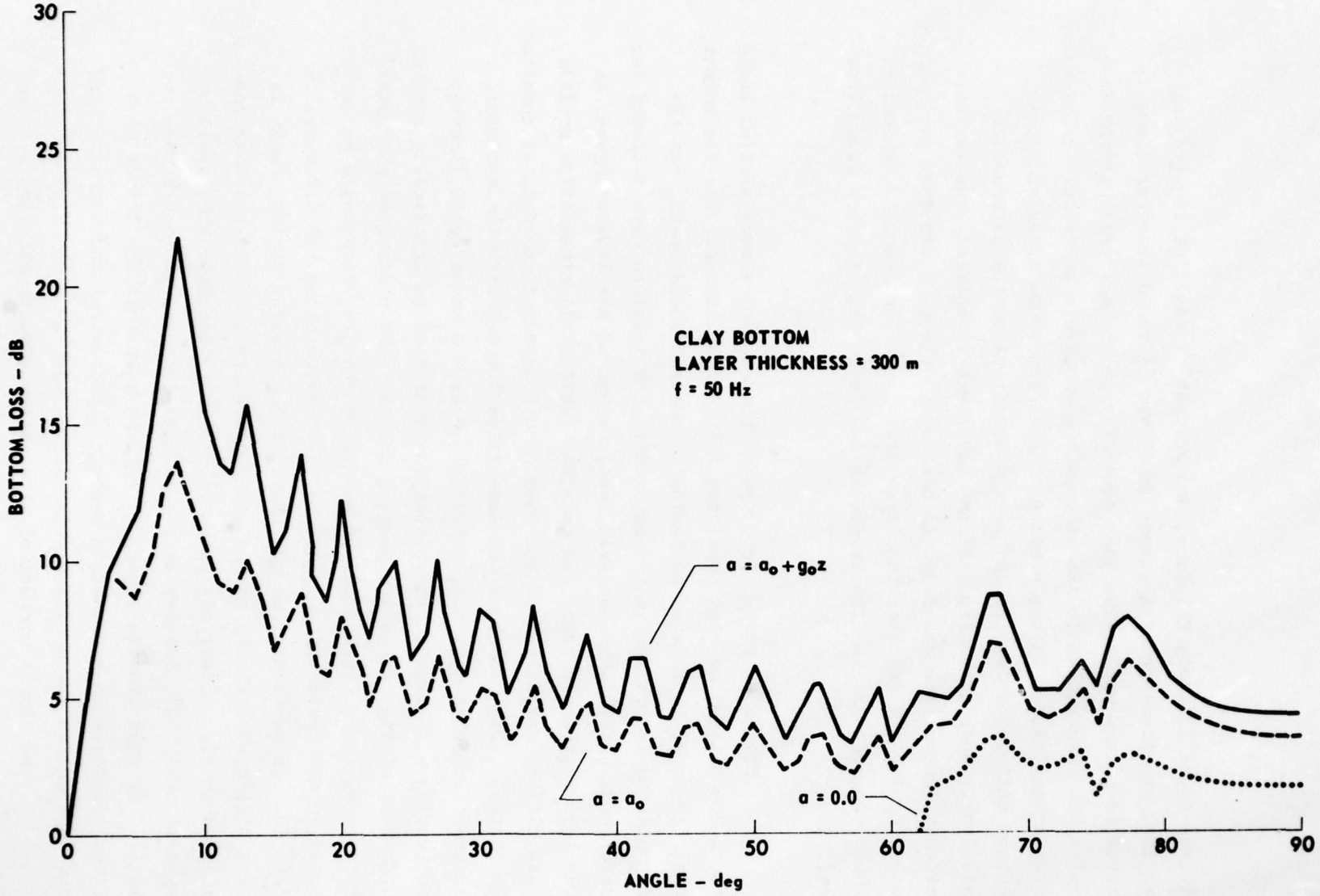

FIGURE 22
COMPUTED BOTTOM REFLECTION LOSS FOR A 300 m CLAY LAYER WITH ZERO SOUND SPEED GRADIENT AND VARIOUS ATTENUATION PROFILES

ARL - UT
AS-77-126 P
WEW - DR
2 - 8 - 77

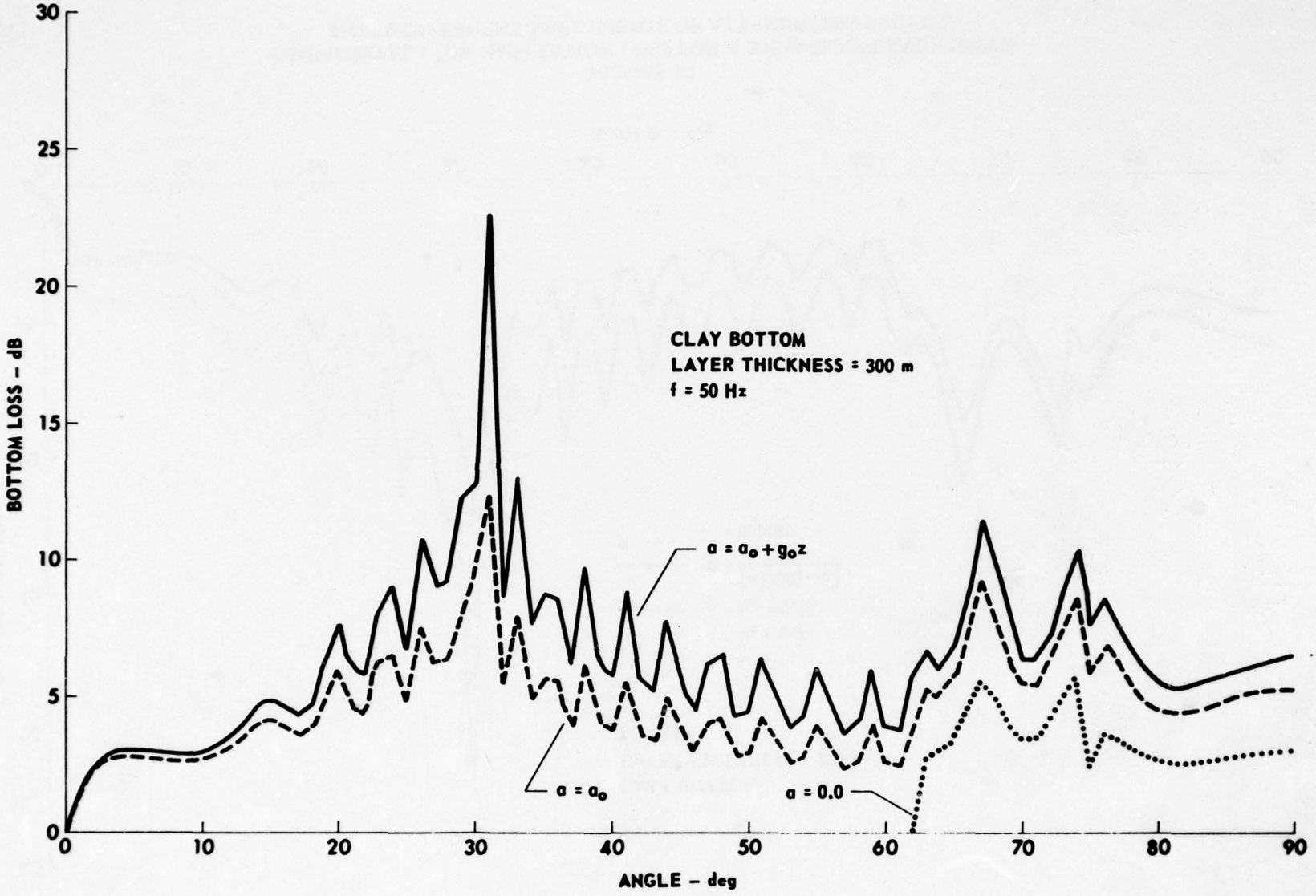

ARL - UT
AS-77-127P
WEW - DR
2-8-77

FIGURE 23
COMPUTED BOTTOM REFLECTION LOSS FOR A 300 m CLAY LAYER HAVING A POSITIVE SOUND SPEED GRADIENT AND VARIOUS ATTENUATION PROFILES

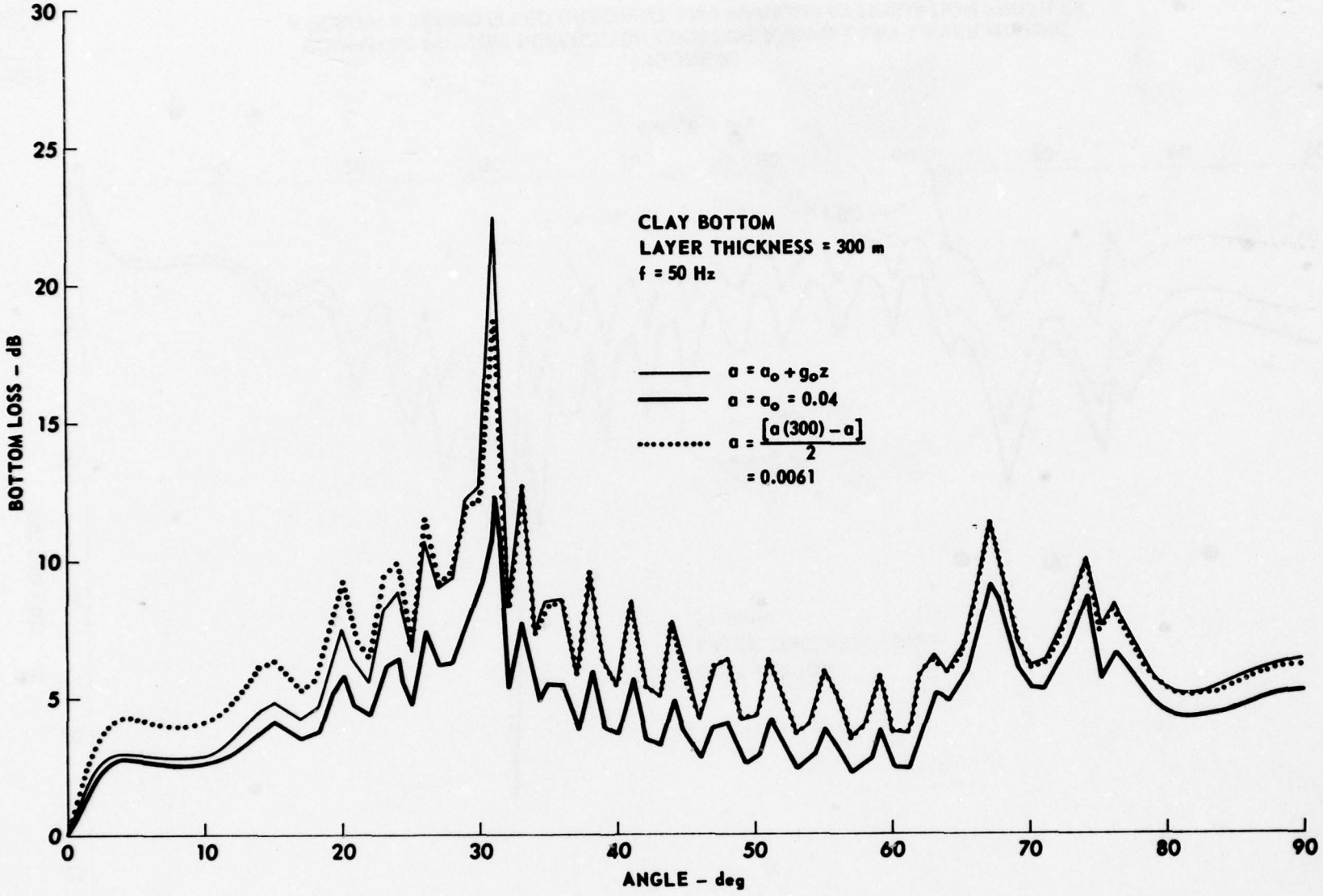

FIGURE 24
COMPUTED BOTTOM REFLECTION LOSS FOR A 300 m CLAY LAYER USING THREE DIFFERENT TREATMENTS OF ATTENUATION PROFILE

ARL - UT
AS-77-130 P
WEW - DR
2 - 8 - 77

we now consider, in addition to the linear attenuation profile and a constant attenuation having the surficial value of 0.004 dB/m, a third case--a constant attenuation having a value equal to the layer average of the linear profile (0.0061 dB/m). Here we see again that, at low grazing angles, the constant surficial value and the linear profile cases are nearly the same, although they differ markedly at high angles. However, in agreement with intuition, the linear profile and the layer average constant profile cases become essentially identical at high angles, although they differ at low angles.

Thus, although the processes contained in the full wave theory treatment used in Figs. 22 through 24 appear superficially to be complex, the overall picture emerging is relatively simple and can be understood on the basis of simple ray path considerations. It should be pointed out that the loss below the basalt shear wave critical angle of 62° is entirely due to absorption, not to propagation of energy into the substrate. This is illustrated by the zero attenuation curves given in Figs. 22 and 23.

All the calculations so far displayed here have concerned a clay type sediment. Even considering the properties of a single sediment layer only, there are a wide variety of common sediment types. Nevertheless, some insight can be gained into effects of attenuation profiles on reflection from other sediments by examining a silt type layer for several treatments of attenuation. Figure 25 shows the bottom reflection loss for a 250 m silt layer, overlying basalt, for three different attenuation gradients ranging from zero to a value considerably in excess of any to be expected in realistic sediments. The surficial attenuation value, $\alpha(0)$, used in the calculations of Fig. 25, was somewhat lower than the nominal value for silt. In Fig. 26 the same calculations are reproduced with the only change being an increase in surficial attenuation by a factor of 4. Thus, these two figures taken together bracket the expected range of both surficial attenuation and attenuation gradient.

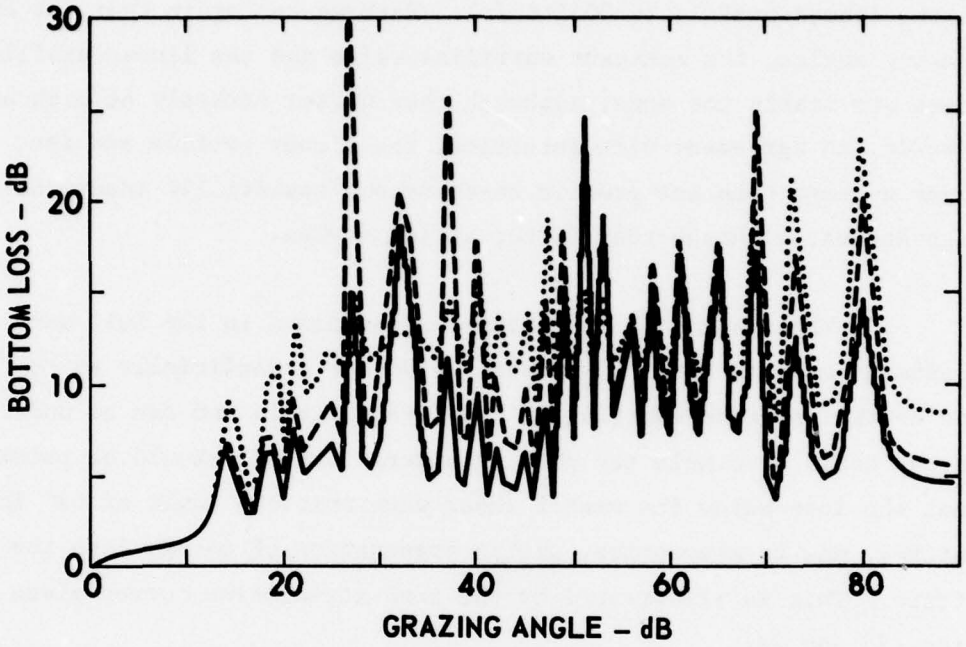

FREQUENCY: 100 Hz

SEDIMENT: SILT

SURFICIAL ATTENUATION: 0.006 dB/m

ATTENUATION GRADIENT:

———— 0 dB/m/m

– – – – – – – 3×10^{-5} dB/m/m

..... 12×10^{-5} dB/m/m

FIGURE 25
COMPUTED BOTTOM REFLECTION LOSS FOR A 250 m SILT LAYER HAVING AN ARTIFICIALLY LOW SURFICIAL ATTENUATION WITH THREE ATTENUATION GRADIENTS

ARL:UT
AS-78-654-P
TLF - GA
4 - 21 - 78

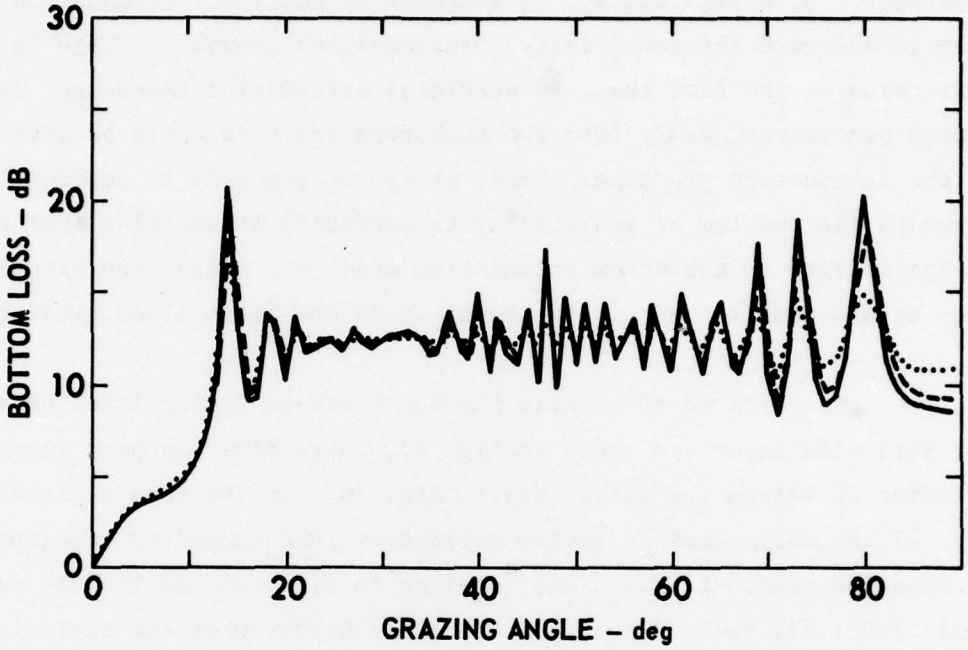

FREQUENCY: 100 Hz

SEDIMENT: SILT

SURFICIAL ATTENUATION: 0.024 dB/m

ATTENUATION GRADIENT:

———— 0 dB/m/m

– – – – – – – 3×10^{-5} dB/m/m

..... 12×10^{-5} dB/m/m

FIGURE 26
COMPUTED BOTTOM REFLECTION LOSS FOR A 250 m SILT LAYER WITH THREE ATTENUATION GRADIENTS

ARL:UT
AS-78-655-P
TLF - GA
4 - 21 - 78

It will be observed that once again the upward refracting effect of the sound speed gradient (1.0 sec^{-1}) results in an insensitivity to attenuation gradient at low angles, although the surficial value is important. More importantly, an increase in surficial attenuation is seen to decrease the sensitivity to attenuation gradient. This is a reflection of the fact that, as surficial attenuation increases, less energy penetrates deeply into the subbottom where it could be affected by the attenuation gradient. Thus, it is not possible to completely separate the problem of sensitivity to surficial attenuation from that of sensitivity to subbottom attenuation gradient. This same situation also occurs with respect to the sound speed and attenuation gradients.

The effects of a still further increase in surficial attenuation for this silt layer are shown in Fig. 27, where $\alpha(0)$ has been increased by a factor of 4 from the value used in Fig. 26. In the case depicted in Fig. 27 the variations in bottom reflection loss caused by changing the attenuation gradient in a manner similar to Figs. 25 and 26 were too small ($\simeq$0.1 dB) to be displayed. In other words, when the surficial attenuation is sufficiently large, the bottom loss becomes completely insensitive to the attenuation gradient.

Finally, a comment concerning the effects of frequency variations on the importance of subbottom attenuation gradients is in order. As frequency increases, subbottom paths are reduced in amplitude due to the increase in absorption with frequency. Therefore, there will be a tendency toward a saturation of the effects of subbottom attenuation, and the total reflected field will be dominated by reflection from the water-sediment interface.

D. Sloping Bottom Studies

This research program has included two studies dealing with propagation in a range variable environment. One, bottom roughness effects, was dealt with in section II.A., and the other, propagation over a sloping bottom, will be summarized in this section.

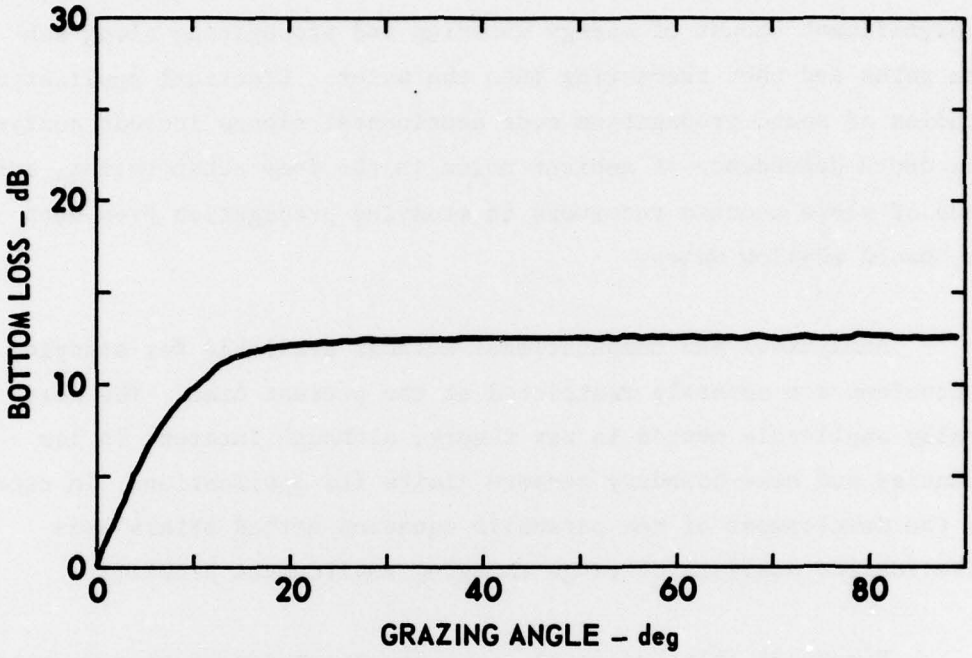

FREQUENCY: 100 Hz

SEDIMENT: SILT

SURFICIAL ATTENUATION: 0.096 dB/m

ATTENUATION GRADIENTS: 0, 3×10^{-5}, 12×10^{-5} dB/m/m

FIGURE 27
COMPUTED BOTTOM REFLECTION LOSS FOR A 250 m SILT LAYER WITH AN ARTIFICIALLY HIGH SURFICIAL ATTENUATION

ARL:UT
AS-78-653-P
TLF-GA
4-21-78

The process of multipath, or mode, conversion is the most characteristic and unique mechanism associated with acoustic propagation up, or down, continental slopes. In addition to this process, which one might think of as essentially geometric in nature, the presence of sloping (tilted) layers of rock and sedimentary material raises the possibility of a significant amount of energy entering and propagating along sub-bottom paths and then reemerging into the water. Practical applications of studies of sound propagation over continental slopes include analysis of the depth dependence of ambient noise in the deep ocean basins, and the use of slope mounted receivers in studying propagation from deep water toward shallow water.

Analytical and computational methods available for studying such problems are severely restricted at the present time. The most generally applicable method is ray theory, although interest in low frequencies and near-boundary sensors limits its application. In recent years the development of the parabolic equation method offers some promise for the analysis of range changing environment problems.

Figure 28 illustrates the most important aspect of propagation from a source in shallow water, over the continental slope, to deep water. A single mid-Pacific sound speed profile having a 700 m axis was used for these calculations. This figure illustrates vividly the multipath conversion process associated with this geometry. As rays propagate outward from the shallow water source, they encounter the slope and suffer a conversion to rays having an angle decrease by twice the slope angle (in this case 4°). Thus, even quite steep rays are quickly converted to angles sufficiently shallow to be trapped in the SOFAR channel, where they remain.

The fundamental geometric nature of this process implies a considerable degree of universality, independent of slope angle, bottom composition, and source depth. It is clear, therefore, that such multipath conversion processes will result in shallow water sources producing

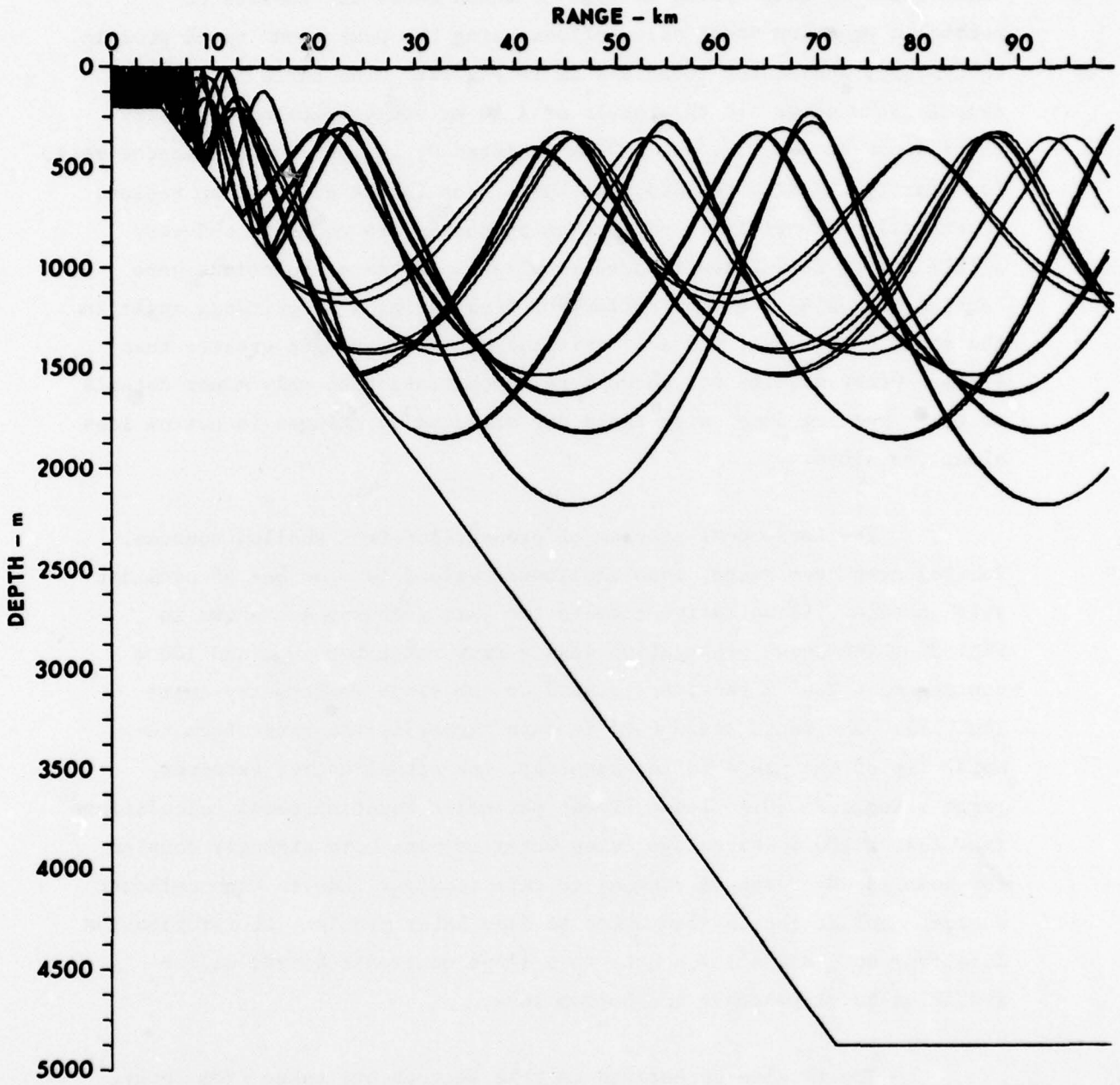

FIGURE 28
NORMAL MODE ATTENUATION COEFFICIENTS versus MODE NUMBER AND EQUIVALENT RAY ANGLE FOR A CLAY LAYER USING THREE DIFFERENT TREATMENTS OF ATTENUATION PROFILE

ARL - UT
AS-77-1197
JAS - GA
10 - 7 - 77

a deep water acoustic field exhibiting a pronounced depth dependence. This effect is illustrated in Fig. 29 which shows the results of parabolic equation model calculations using the same sound speed profile, bathymetry, and source locations as in Fig. 28. The three 50 Hz calculations shown are the result of a 10 km range averaged intensity carried out at 50, 100, and 150 km (shifted 0, 10, and 20 dB, respectively, for clarity). These results show that, even in the 45 to 55 km region, essentially all multipath conversion processes are complete and very little energy is coupled to deep receivers. These calculations were carried out using a bottom reflection loss having a 4° critical angle in the range 0 to 67 km, and a 1° critical angle for ranges greater than 67 km. Other studies not shown here demonstrate that only minor details of the resulting deep water field are affected by changes in bottom loss along the slope.

The reciprocal problem of propagation from shallow sources, located over deep water, into shallower regions is also one of considerable concern. Illustrative results for this geometry are shown in Fig. 30 which shows propagation loss versus range for 10 m and 100 m sources to a 2000 m receiver located on the slope (bathymetry as in Fig. 28). The range scale used in this figure is the range from the upper lip of the slope to the receiver, the actual source receiver range being some 30 km less. These parabolic equation model calculations show that a 100 m source over deep water is much more strongly coupled (by some 18 dB at longer ranges) to this receiver than is the shallower source. Unlike the shallow water to deep water problem, the propagation loss from such a shallow source to a slope mounted receiver will be sensitive to slope angle and bottom loss.

The results summarized in this section are taken from Focke,[13] where more complete details of this study are discussed.

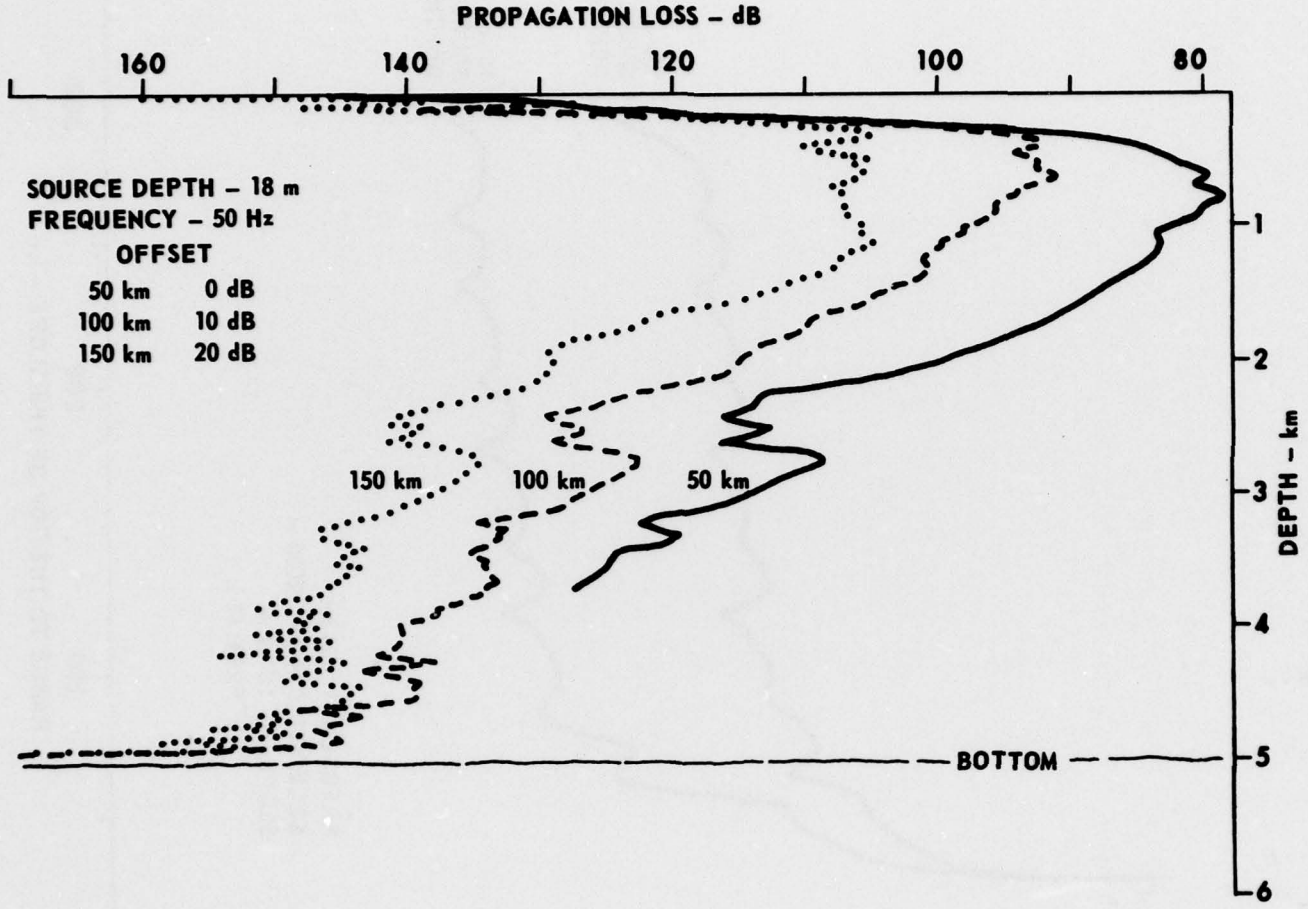

FIGURE 29
RANGE AVERAGE PROPAGATION LOSS versus DEPTH AT THREE RANGES

ARL:UT
AS-78-1685
KEH - GA
10-31-78

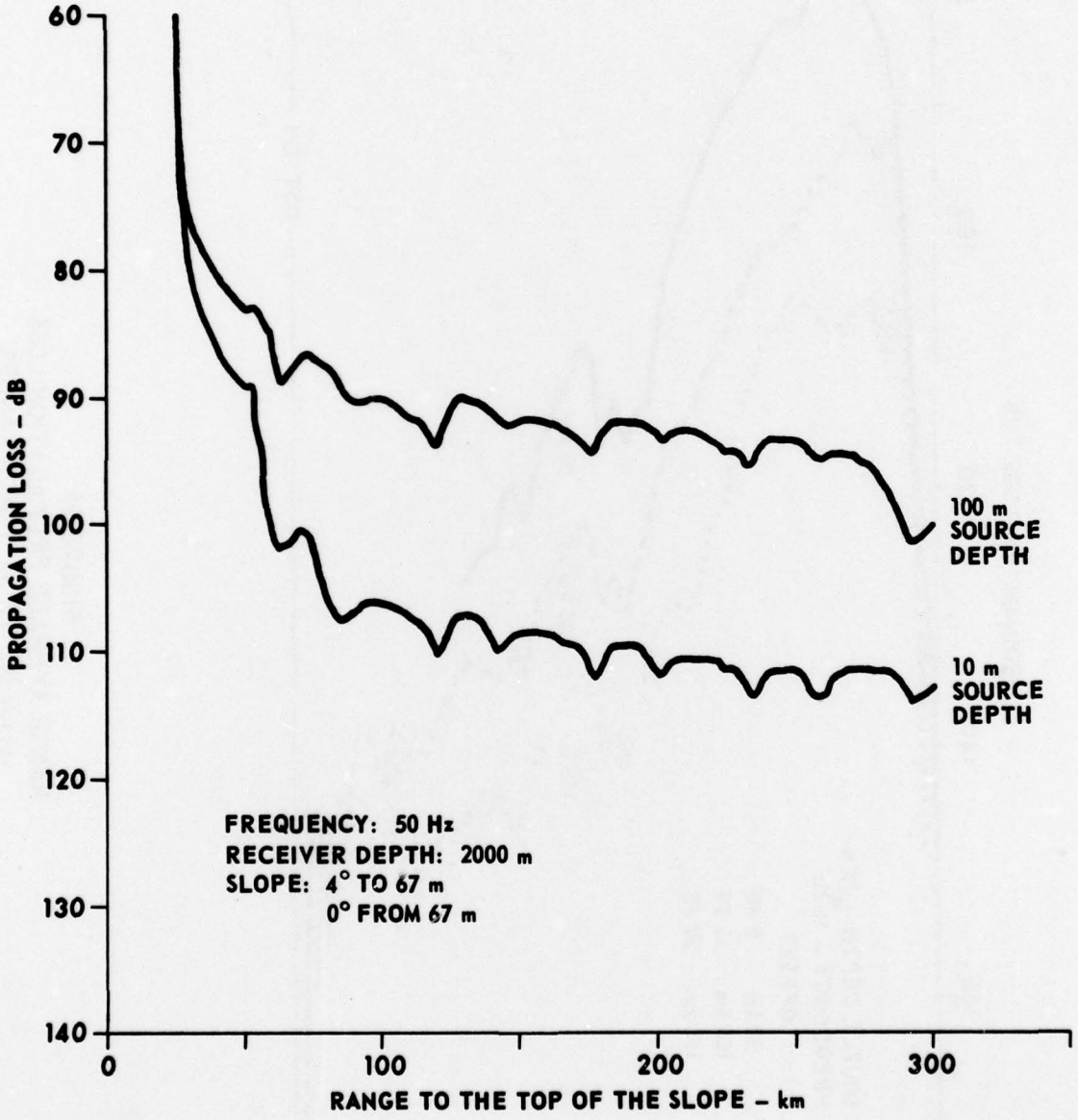

FIGURE 30
AVERAGE PROPAGATION LOSS versus RANGE FOR A 2000 m SLOPE MOUNTED RECEIVER AND TWO SOURCE DEPTHS

ARL:UT
AS-78-1684
KEH - GA
10 - 31 - 78

E. Shallow Water Propagation

The objective of a task under this contract directed toward an examination of shallow water propagation problems was to determine which aspects of the deep water bottom interaction problem may carry over to shallow water problems. Certainly the basic bottom interaction (local) processes of refraction, reflection, scattering, absorption, and compressional-shear conversion are qualitatively the same as in deep water. However, the structure of sediments is substantially different in shallow water due to the presence of different sediment types, temperature, deposition rates, pressure, currents, and other factors. As a result, certain situations, such as deep refraction of acoustic energy through undisturbed thick clay layers, do not arise in shallow water where sand and rock bottoms are more common and layering tends to be more affected by the scouring action of currents (rivers, tides, wave action, etc.).

From the point of view of bottom interaction, shallow water propagation problems are most distinctly differentiated from deep water problems by two considerations, (1) energetics of water-subbottom propagation and (2) sediment types and structure.

At a fixed frequency and for constant subbottom composition, a reduction in water depth results in an increase in the fraction of energy transported within the bottom. This process is especially important at low frequencies where a sufficient reduction in water depth results in a total absence of nonbottom interaction paths, even in the presence of a near-surface positive sound speed gradient (surface duct). Computations made using the normal mode model developed under this contract for deep water use confirm this expectation. A consequence of this increase in bottom interacting energy is an increased sensitivity to bottom parameter variations and uncertainties.

Accompanying this increase in the importance of bottom interaction in shallow water is a change in the important subbottom

parameters resulting from different sediment composition. The common occurrence of hard, low porosity sediments, such as sand, leads to a decrease in the importance of sound speed and density gradients (see Hawker, Focke, and Anderson[11] and Rutherford and Hawker[7]). These same hard sediments also result in the increased likelihood that scattering will be an important process. The common occurrence of thin sediments overlying rock layers will increase the importance of both compressional-shear wave conversion processes as well as the likelihood of excitation of Stoneley waves.[8]

F. Modeling Support

Improvements in several commonly used models were carried out during the present year.

The ARL:UT normal mode model NEMESIS was upgraded to decrease execution time and reduce the requirements for user interaction. In addition, a newly developed method for computing mode group velocities was implemented, resulting in a threefold reduction in execution time and several orders of magnitude improvement in accuracy.

The ARL:UT bottom reflection loss model, BOTLOSS, was extended so that the geoacoustic parameters (density, sound speed, and attenuation) could be introduced pointwise (discretely) with linear interpolation between the points. This method replaces the two- and three-parameter functional descriptions used previously. A paper documenting the procedures used in this model has been prepared for publication (Hawker and Foreman[12]).

The family of ARL:UT ray trace models collectively known as RANGER, developed for use in this research program, was documented during this contract year in a report by Foreman.[14]

REFERENCES

1. W. A. Kuperman, "Coherent Component of Specular Reflection and Transmission at a Randomly Rough Two-Fluid Interface," J. Acoust. Soc. Am. 58, 365 (1975).

2. S. R. Rutherford, K. E. Hawker, and S. G. Payne, "A Study of the Effects of Bottom Roughness on Low Frequency Sound Propagation," to be published in J. Acoust. Soc. Am.

3. K. E. Hawker, "An Introduction to the Acoustic Processes of Bottom Interaction with Applications to Surveillance" (U), Applied Research Laboratories Technical Report No. 77-20 (ARL-TR-77-20), Applied Research Laboratories, The University of Texas at Austin, April 1977. CONFIDENTIAL

4. J. A. Shooter, K. E. Hawker, and L. D. Hampton, "An Introduction to the Characteristics and Acoustic Mechanisms of the Deep Ocean Ambient Noise Field" (U), Applied Research Laboratories Technical Report No. 77-55 (ARL-TR-77-55), Applied Research Laboratories, The University of Texas at Austin, September 1977. CONFIDENTIAL

5. D. F. Gordon, "Theoretical Propagation of Low Frequency Sound in the Deep Ocean and its Interaction with the Bottom" (U), NUC-TP-536, U. S. Naval Ocean Systems Center, San Diego, California, January 1977. CONFIDENTIAL

6. E. L. Hamilton, "Geoacoustic Models of the Sea Floor," in Physics of Sound in Marine Sediments, L. D. Hampton (ed.) (Plenum Press, New York, 1973).

7. S. R. Rutherford and K. E. Hawker, "The Effects of Density Gradients on Bottom Reflection Loss for a Class of Marine Sediments," J. Acoust. Soc. Am. 63, 750 (1978).

8. K. E. Hawker, "The Influence of Stoneley Waves on Plane Wave Reflection Coefficients: Characteristics of Bottom Reflection Loss," J. Acoust. Soc. Am. 64, 548 (1978).

9. K. E. Hawker, "The Existence of Stoneley Waves as a Loss Mechanism in Plane Wave Reflection Problems," to be published in J. Acoust. Soc. Am.

10. K. E. Hawker, W. E. Williams, and T. L. Foreman, "A Study of the Acoustical Effects of Subbottom Absorption Profiles," to be published in J. Acoust. Soc. Am.

11. K. E. Hawker, K. C. Focke, and A. L. Anderson, "A Sensitivity Study of Underwater Sound Propagation Loss and Bottom Loss," Applied Research Laboratories Technical Report No. 77-17 (ARL-TR-77-17) Applied Research Laboratories, The University of Texas at Austin, February 1977.

12. K. E. Hawker and T. L. Foreman, "A Plane Wave Reflection Loss Model Based on Numerical Integration," submitted for publication in J. Acoust. Soc. Am.

13. K. C. Focke, "Effects of the Continental Slope on the Modeling of Propagation Loss," in preparation.

14. T. L. Foreman, "Acoustic Ray Models Based on Eigenrays," Applied Research Laboratories Technical Report No. 77-1 (ARL-TR-77-1), Applied Research Laboratories, The University of Texas at Austin, January 1977.

7 December 1978

DISTRIBUTION LIST FOR
ARL-TR-78-49
UNDER CONTRACT N00039-77-C-0003, ITEM 0001
UNCLASSIFIED

Copy No.

Commanding Officer
Naval Electronic Systems Command
Department of the Navy
Washington, DC 20360
1 Attn: J. Cybulski, Code 320
2 Code PME-124-30
3 Code PME-124-60

4 Office of Naval Research
Branch Office Chicago
536 South Clark Street
Chicago, IL 60605

Commanding Officer
Naval Ocean Research and Development Activity
NSTL Station, MS 39529
5 Attn: M. G. Lewis, Code 500
6 J. Matthews, Code 360
7 G. Morris, Code 340

Naval Research Laboratory
Department of the Navy
Washington, DC 20375
8 Attn: Code 8160

Commanding Officer
Naval Ocean Systems Center
Department of the Navy
San Diego, CA 92152
9 Attn: H. P. Bucker, Code 5311
10 E. L. Hamilton

Chief of Naval Material
Department of the Navy
Washington, DC 20360
11 Attn: CDR E. Young, Code 08T24

Superintendent
Naval Postgraduate School
Monterey, CA 93940
12 Attn: Library

Distribution List for ARL-TR-78-49, N00039-77-C-0003, Item 0001 (Cont'd)

Copy No.

Chief of Naval Operations
Department of the Navy
Washington, DC 20362
13 Attn: R. S. Winokur, OP-095E

Commanding Officer
Office of Naval Research
800 N. Quincy Street
Arlington, VA 22217
14 Attn: J. B. Hersey, Code 102-OS
15 A. O. Sykes

Commander
Naval Sea Systems Command
Department of the Navy
Washington, DC 20362
16 Attn: C. D. Smith, Code 06H1

17 - 28 Commanding Officer and Director
Defense Documentation Center
Defense Services Administration
Cameron Station, Building 5
5010 Duke Street
Alexandria, VA 22319

29 Office of Naval Research
Resident Representative
Room No.582
Federal Building
Austin, TX 78701

30 Glen E. Ellis, ARL:UT

31 Loyd D. Hampton, ARL:UT

32 Kenneth E. Hawker, ARL:UT

33 Steven K. Mitchell, ARL:UT

34 Clark Penrod, ARL:UT

35 Steven R. Rutherford, ARL:UT

36 Jack A. Shooter, ARL:UT

Distribution List for ARL-TR-78-49, N00039-77-C-0003, Item 0001 (Cont'd)

Copy No.

37	Paul J. Vidmar, ARL:UT
38	Library, ARL:UT
39 - 62	Reserve, ARL:UT